University College of Southeast Norway
Faculty of Technology, Natural Sciences and Maritime Sciences
—
Doctoral dissertation no. 25
2017

Åsmund Sandvand

High-stability piezoresistive pressure sensors

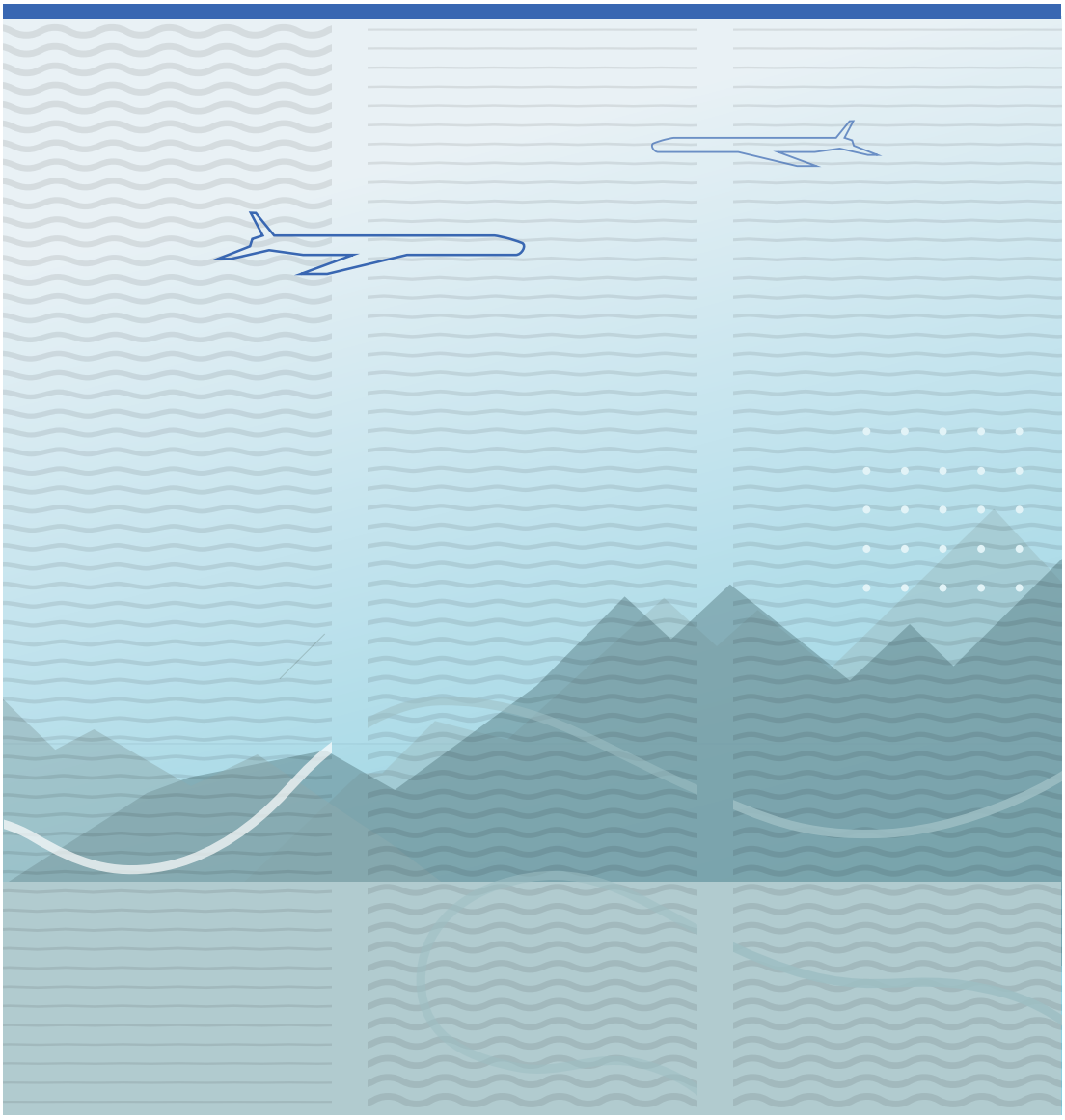

HSN

Åsmund Sandvand

High-stability piezoresistive pressure sensors

A PhD dissertation in
Applied Micro- and Nanosystems

Faculty of Technology, Natural Sciences and Maritime Sciences
University College of Southeast Norway
Kongsberg, 2017

Doctoral dissertations at the University College of Southeast Norway no. 25

ISSN: 2464-2770 (print)
ISSN: 2464-2483 (electronic)
ISBN: 978-82-7860-304-8 (print)
ISBN: 978-82-7860-305-5 (electronic)

Print: University College of Southeast Norway

Preface

This thesis is submitted in partial fulfilment of the requirements for the degree of Philosophiae Doctor (Ph.D.) at the University College of Southeast Norway (USN).

The study was conducted from September 2013 to March 2017 at the Department of Micro- and Nano Systems Technology (IMST). Professor Einar Halvorsen was the main supervisor, with Professor Knut E. Aasmundtveit and Professor Henrik Jakobsen as co-supervisors.

The work was part of a collaboration between USN and MEMSCAP AS, supported by the Research Council of Norway through the project *Precision Piezoresistive Pressure-sensor Platform* (4P) under Grant 228755. Additional support was given through the Norwegian Micro- and Nano-Fabrication Facility, NorFab under Grant 197411/V30 and the Norwegian PhD Network on Nanotechnology for Microsystems under Grant 221860/F40.

I would like to thank my supervisors Professor Einar Halvorsen, Professor Knut E. Aasmundtveit and Professor Henrik Jakobsen for their support and valuable discussions during this work. Also thanks to the other people at IMST.

A special thanks to Executive Chairman Jan Hallenstvedt at MEMSCAP for support and encouragements during the project. Thanks also to my other colleagues at MEMSCAP for their support and assistance in manufacturing of the test sensors, and to project partner Sigurd Moe at SINTEF MiNaLab.

Finally, a special thanks to my wife Karin and my family for encouragements and support during this work.

Abstract

Piezoresistive pressure sensors have been in use for decades and are among the most successful micromachined sensors. From their introduction in the 1960s, they have experienced a dramatic improvement on performance and stability, as new microfabrication techniques have been developed. For high-accuracy avionic applications, there is a strong focus on the long-term stability of the sensor output-signal. Higher stability makes increased service-intervals possible and open the doors to new applications areas. This thesis focuses on possible root causes influencing the stability for piezoresistive pressure sensors. Although the main focus has been on the SP82-design from MEMSCAP, the results are relevant also for other sensor designs using similar packaging technologies.

It has been found that even small amounts of excess glass frit material in the die lamination process may cause a major influence on the sensor zero point and temperature sensitivity. High residual stress in the excess glass frit volume will also result in increased risk for mechanical stress release in the form of microcrack formation. By optimizing the glass frit distribution, the influence from the die lamination on the sensor output-signal has been reduced and the stability has been improved.

Another major finding has been that the use of a thermoset polymer as a die-attach material might result in an unwanted signal drift when the sensors are stored for weeks under ambient environmental conditions. This was found to be caused by diffusion of water into the polymer, leading to spatially localized swelling with resulting mechanical stress changes, combined with physical aging. A new support die design has been designed and tested, reducing this effect to neglectable levels.

The sensitivity of a sealed sensor structure to changes in the sensor cap pressure has been modelled and experimentally verified. Examples of resulting influence from various storage conditions on signal drift as well as characteristic over temperature are demonstrated, and resulting hermeticity requirements are discussed.

A new metallization pattern for *in situ* observation of metal properties in a piezoresistive pressure sensor has been developed and initial testing has been performed. By limiting the design change to the metal mask only, this provides a cost effective approach for characterizing of metal properties where the test structure can be combined with functional devices on the same wafer.

List of publications

Articles omitted from online publication due to publishers' restrictions

1. Å. Sandvand, E. Halvorsen and K.E. Aasmundtveit, "Finite element modelling of influence of bonding material distribution in precision piezoresistive MEMS pressure-sensors", *Electronics System-Integration Technology Conference (ESTC)*, Helsinki, Finland, 16-18 September 2014, DOI: 10.1109/ESTC.2014.6962829

2. Å. Sandvand, E. Halvorsen, K.E. Aasmundtveit and H. Jakobsen, "Influence of sensor-package hermeticity-level on long-term drift for a piezoresistive MEMS pressure-sensor", *Microelectronics Packaging Conference (EMPC)*, Friedrichshafen, Germany, 14-16 September 2015

3. Å. Sandvand, E. Halvorsen, K.E. Aasmundtveit and H. Jakobsen, "Influence of Glass-Frit Material Distribution on the Performance of Precision Piezoresistive MEMS Pressure Sensors", *IEEE Transactions on Components, Packaging and Manufacturing Technology (TCPMT),* Volume 5, Issue 11 (2015), Pages 1559-1566, DOI: 10.1109/TCPMT.2015.2486018

4. Å. Sandvand, E. Halvorsen, K.E. Aasmundtveit and H. Jakobsen, "Identification and elimination of hygro-thermo-mechanical stress-effects in a high-precision MEMS pressure sensor", *IEEE Journal of Microelectromechanical Systems (JMEMS)*, Volume 26, Issue 2 (2017), Pages 415-423, DOI:10.1109/JMEMS.2017.2651162

5. Å. Sandvand, E. Halvorsen and H. Jakobsen, "*In situ* observation of metal properties in a piezoresistive pressure sensor", accepted for publication in *IEEE Journal of Microelectromechanical Systems (JMEMS)* DOI:10.1109/JMEMS.2017.2747090

Abbreviations

%FS	Percentage of Full Scale
CT	Computed Tomography
CTE	Coefficient of Thermal Expansion
DRIE	Deep Reactive Ion Etch
DWB	Direct Wafer Bonding
FEA	Finite Element Analysis
FET	Field Effect Transistor
MEMS	Micro Electro Mechanical System
MOS	Metal Oxide Semiconductor
NEG	Non-Evaporable-Getter
ppm	Parts per million (1 ppm = 0.0001 %)
RGA	Residual Gas Analysis
RVSM	Reduced Vertical Separation Measurements
SCR	space charge region
SOI	Silicon On Insulator
TCO	Thermal Coefficient of Offset
TCS	Thermal Coefficient of Sensitivity
TCR	Temperature Coefficient of Resistivity
T_g	Glass transition temperature

ZP	Zero Point
V_{FB}	Flatband voltage
V_{TH}	Threshold voltage

Table of Contents

Articles omitted from online publication due to publishers' restrictions

1 Introduction

Pressure sensors using piezoresistive elements in silicon as the stress sensitive element were first introduced in the 1960s, and are among the most successful micromachined sensors. Since then, a number of new microfabrication techniques have been introduced, improving the performance of piezoresistive pressure sensors [1]. With this improved performance, the piezoresistive pressure sensors have been introduced in a number of advanced applications with high demands on both precision as well as stability, such as medical and automotive applications as well as applications for the avionics market.

For the avionics market, the decreasing atmospheric pressure versus altitude is used for calculating flight altitude based on pressure measurements. This is done by an *absolute type* pressure sensor, where the pressure is measured relative to a vacuum reference. In addition, the air-speed can be calculated by measuring the difference between the total incoming air-pressure (stagnation-pressure) and the atmospheric pressure (static pressure). This is done by a *differential type* pressure sensor, measuring the difference between two pressures. The air-speed can be different from the speed over ground due to strong winds at the flight altitude, but the air-speed measurement is extremely important for operating the aircraft within safe limits. Too low airspeed will cause the aircraft to stall, while too high airspeed might result in structural damage to the aircraft.

There are several different units for pressure used in the industry depending on application and geographic location. In this thesis, we use the SI-unit Pascal (P) where 100 kPa = 1 bar and 1 hPa = 1 mbar. One standard atmosphere (atm) is a constant that is used for describing typical atmospheric pressure at sea level on earth. Disregarding influence from weather systems, the standard atmosphere on earth is defined as 1013.25 hPa at sea level. As we move upwards from sea level, the air pressure will decrease. At an altitude of 1000 meters, the air pressure has decreased to 0.89 atm or

901.79 hPa. At a maximum flight altitude of 12500 m, the air pressure has decreased to 0.18 atm or 178.65 hPa.

1.1 Background

MEMSCAP has long experience in the field of piezoresistive pressure, both for the highly demanding avionic market as well as for medical devices. This involves design of basic pressure sensing elements and sensors, as well as complete calibrated sensor modules, containing pressure sensors with accompanying electronics needed to deliver digitized and compensated pressure reading for various applications. Extensive work has been focused on algorithms for compensation of temperature and non-linearity effects. By implementing and optimizing advanced algorithms for signal compensation, it has become clear that further improvements are not possible without a thorough analysis of the basic sensor design, identifying root causes to observed anomalies and reducing these effects.

The baseline high-precision pressure-sensors contained in this work are named the SP82 family and are typically used for avionic applications such as air-data computers and airplane cabin pressure monitoring, providing pressure measurements for calculating air-speed and altitude for a high number of airplane systems. Figure 1 shows the SP82 pressure sensor and some calibrated sensor module variants. Due to its high reliability and accuracy, the SP82 sensors are also used for other highly demanding applications such as the Tunable Laser Spectroscope (TLS) on the Mars Science Laboratory mission's Curiosity rover [2] and the Carmat artificial heart prosthesis [3].

The initial mechanical design concept of the present SP82 configuration, with the die-stacking and applying pressure through a glass tube to the electrically inactive side of the sensor die, origins from work at SINTEF during the 1970s. In 1986, the stability was improved by work at Sensonor, with the design of a new sensor die with buried piezoresistors. Incremental design improvements further improving the stability has also been done at MEMSCAP.

The long-term stability of SP82 is currently specified as 0.02 %FS/year (% of Full Scale/year). For 1mA DC excitation, typical zero-point is specified as ±10mV, Full Scale Output (FSO) is 125 mV ±35%, Temperature Coefficient of Offset (TCO) is ±0.07 %FS/°C and Temperature Coefficient of Sensitivity is 0.01 ±0.01%/°C. Both maximum operating temperature and maximum storage temperature are -55 °C to +125 °C.

When the sensor is calibrated in a sensor module, a total inaccuracy of less than ±0.05 %FS is typically obtained for the full pressure range over a temperature range of -40 °C to +85 °C.

Figure 1 The SP 82 pressure sensor and calibrated sensor modules

Total accuracy requirements for the most demanding aerospace applications can be one to two orders of magnitude higher than for industrial and automotive applications. For these applications, there is also a strong focus on identifying the root cause of observed deviations from specifications. When abnormal behavior is identified for commercial applications, a claim can be met by simply giving a customer a replacement unit without a detailed investigation of the root cause of the abnormal behavior. This will influence on the manufacturing yield, but no detailed investigation of the root cause is needed. For avionic applications, the focus is not on the cost of sending a replacement unit, but rather on the investigation on the fundamental root cause of the abnormal behavior. A detailed knowledge of possible factors influencing the performance is therefore needed, and all physical effects influencing the sensor

performance need to be known in detail. Even though the SP82 sensor family is regarded as a high-precision sensor design with a significant market share, the market always strives for even higher accuracies and a better long-term stability.

For the avionic industry, the introduction of the RVSM (Reduced Vertical Separation Measurements) requirements [4] requires accuracy-performance towards 100 ppm of full scale (FS). For a pressure sensor with a FS of 100 kPa, 100 ppm of FS corresponds to 0.1 hPa. When converting atmospheric pressure differences to altitude, this corresponds to an altitude change of 0.8 m at sea level. However, when an aircraft cruises at 45000 feet (13716 m), 0.1 hPa corresponds to an altitude difference of 4.0 m.

In 2013, MEMSCAP decided to address this task through a research project supported by the Norwegian Research Council (NRC). The project was named *4P – Precision Piezoresistive Pressure-sensor Platform*, and this Ph.D. work has been a central part of this project.

1.2 Research goals and approach

The ultimate goal of this work has been on improving the current state of the art for piezoresistive pressure sensors to have the markets lowest long-term drift of less than 100 ppm of FS per year including thermal hysteresis effects.

The work has focused on physical properties influencing the stability of piezoresistive pressure sensors, in particular on high precision sensors for the avionic market.

The output signal of a pressure sensor is ideally a function of the measured test pressure only. In practical implementations, the output signal is also influenced by a number of other effects. This includes electrical drift in the piezoresistors and interconnect system, mechanical stress in the sensor structure, leakage related phenomena as well as other possible influences. Due to the high number of possible sources, great care should be taken in order to isolate the various contributions.

During the project we have therefore designed and built a number of different test sensors, each focused on a specific failure mode. In addition, the test structures have been modelled using finite element analysis (FEA) in order to calculate the effect of various failure modes and process variations. The modelled behavior has been compared with a large number of measurements on test samples, performed over a variety of temperatures and humidity levels.

During normal sensor manufacturing at MEMSCAP, a number of measurements are done and the results are stored in databases. By doing targeted searches in this data and compare against measurements from test samples, further insight in the importance of various contributing factors to the final sensor accuracy has been found.

The output signal of a piezoresistive pressure sensors is highly temperature dependent. In order to achieve the required accuracies, a flexible approach to signal compensation is needed. We have therefore built a software platform, where MEMSCAP is able to use a number of different recorded signal sequences as input to a variety of temperature and pressure compensation algorithms. By studying the difference signal from the mathematical models, it is thus possible to extract detailed behavior variations from the recorded signals sequences.

1.3 Impact of results

This work has been done in close collaboration with MEMSCAP, which manufactures high-precision pressure sensors and calibrated pressure modules for the avionics market. The present high-precision pressure sensor family is named SP82 and possible improvements to the SP82 pressure sensor family has been focused in this research. Important sensor improvements based on this research has been presented to key customers of MEMSCAP during the project duration and some improvements have already been implemented in the sensor production. Based on this research, MEMSCAP is now able to manufacture pressure sensors with an improved accuracy and stability, and performance variations due to the studied phenomena can be controlled. Deviations from ideal behavior, previously observed by both MEMSCAP and

customers, can now be understood and explained. Although many of these effects might seem minor in magnitude, they cause a limit of the achievable accuracy level for calibrated pressure sensor modules.

At the application level, the improved performance will result in improved altitude and air-speed control for the aircraft equipment-installations using this sensor.

1.4 Structure of the Thesis

The thesis is organized in 5 parts, including this introductory section.

Section 2 contains an introduction of the basic device physics for the piezoresistive pressure sensor used in this work.

Section 3 continues with a detailed description of the various causes that may influence the long-term stability of piezoresistive pressure sensors.

Section 4 contains an overview of contributions of this work

Section 5 contains some concluding remarks

The publications of this work are attached at the end of the thesis as Article I to Article V

2 The piezoresistive pressure-sensor

A traditional silicon pressure-sensor design uses a thin micromachined diaphragm that is deflected due to an applied pressure. The deflection results in high mechanical stress along the edges of the diaphragm, and this stress is detected by stress sensitive piezoresistors placed at positions of maximal mechanical stress. Figure 2 shows a principal sketch of the mechanical design of the absolute pressure sensor used in this work, consisting of three bonded silicon dies mounted into a TO-8 package. A TO-8 package (Transistor Outline, Case style 8) is a metal can package that is hermetically sealed with a welded cap and glass sealed connecting pins.

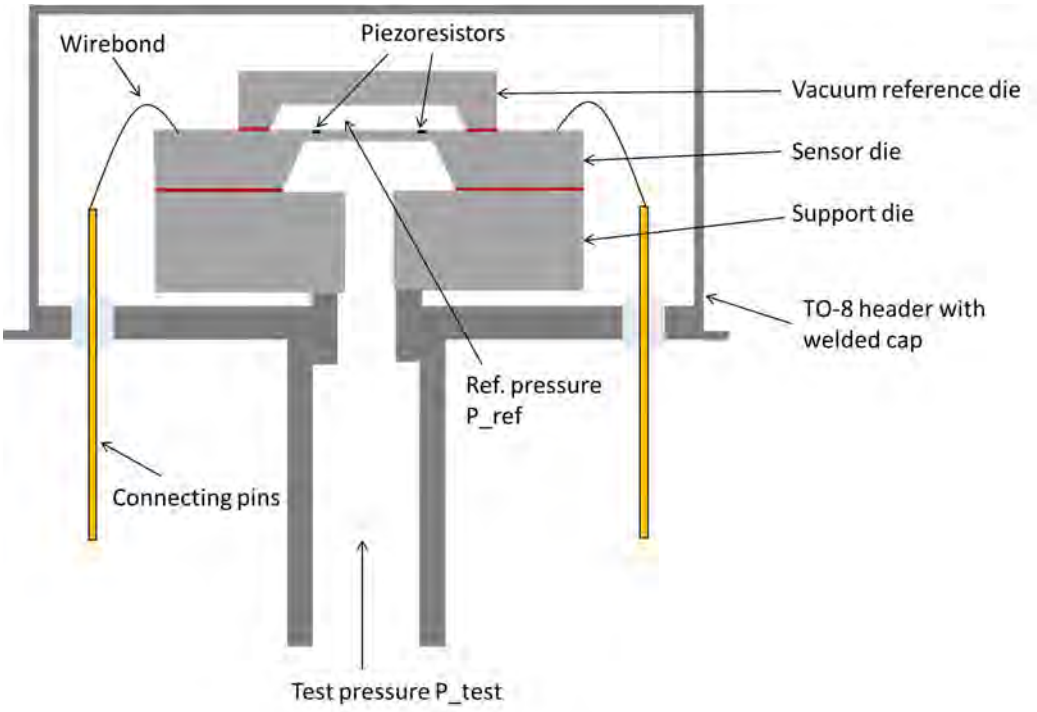

Figure 2 Cross section sketch of piezoresistive pressure sensor

There are a lot of possible design variants of piezoresistive pressure-sensors. Some designs use glass instead of silicon for the vacuum reference die and/or the support die, and the die-bonding technology will vary, but glass frit bonding or anodic bonding are mostly used. The etching of the thin diaphragm can be done by anisotropic etching

for a certain time, or by more advanced thickness control such as etch stop at a buried silicon dioxide layer or at a pn-junction [1].

The central sensor die in Figure 2 contains the diaphragm with piezoresistors and additional metallization needed to form a complete measurement bridge circuit. An example is shown in Figure 3, where the resistors (labelled R1 to R4) are configured as an open Wheatstone bridge. Electrical connections are provided via glass-sealed connecting pins connected with the sensor die using wire bonding. At the wire-bonding stage, the bridge can be closed, or it can be left open at one end to provide for a more flexible electrical compensation approach using external components. In addition to the four resistors at the diaphragm edge, additional resistors are located outside the diaphragm area for accurate temperature measurements. Temperature measurement close to the stress-sensitive piezoresistors is important for accurate temperature compensation of the signal.

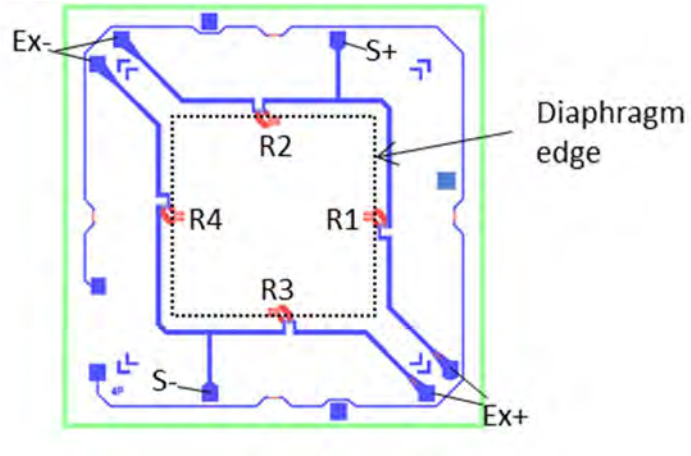

Figure 3 Example of a sensor die layout (top view) with four piezoresistors connected with metal. Red: P+ implant, Blue: Al metal

The cavity between the vacuum reference die and the sensor die is evacuated during manufacturing, forming a vacuum reference for absolute pressure measurements. The support die offers a rigid support of the sensor die and acts as a physical interface to the test pressure port.

A differential pressure sensor can be built by omitting the vacuum reference die and adding a second pressure port to the welded cap.

Figure 4 shows additional details for a 1 bar (100 kPa) sensor die, illustrating typical dimensions and piezoresistor positions. Other pressure ranges can be realized by changing the diaphragm thickness and area.

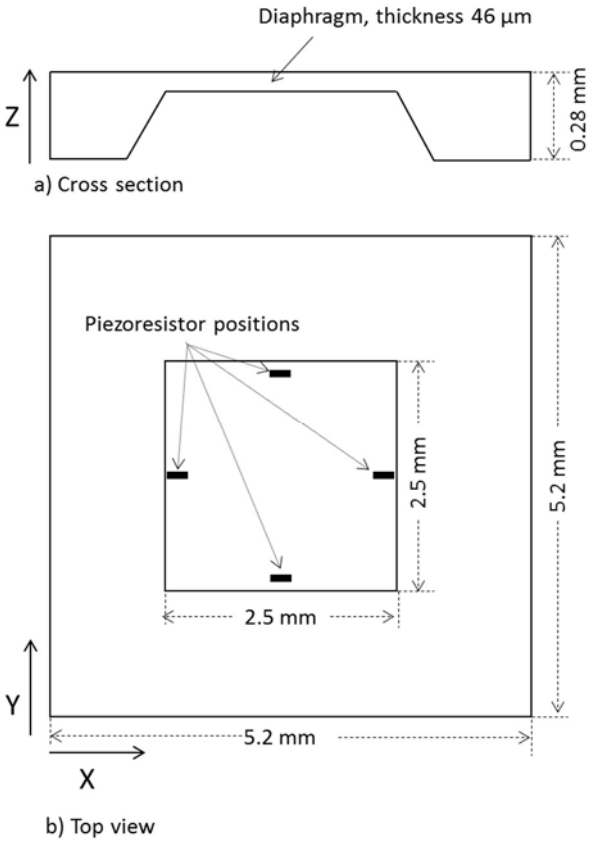

Figure 4 Sensor die with piezoresistor positions

2.1 The sensor die

Silicon has a long tradition as a semiconductor material used for construction of planar electronic devices with a high number of processes and manufacturing equipment available. Development of etching technologies during the 1960's made it possible to also include diaphragm structures in the same die for construction of micro electro mechanical systems (MEMS) devices.

Monocrystalline silicon has near ideal elastic properties and has been extensively used as the main building material for piezoresistive pressure sensors. The following sections contain a short introduction to some basic properties and concepts used for construction of silicon based piezoresistive sensor dies.

2.1.1 Mechanical properties of silicon

Monocrystalline or single-crystal silicon has the silicon atoms ordered in a periodic structure where each atom is attached to four neighbor atoms in a diamond lattice crystal structure. This structure has a cubic repeating element and is therefore called a cubic material. Silicon has anisotropic elastic properties where the Young's modulus depends on which crystal direction of the material that is being deformed, and it is therefore essential to define which crystal direction that is being used.

The various crystal directions are indicated using Miller indexes. The sensor die surface in this work is aligned with the commonly used (100) plane, with the local x and y-axes along the <110> directions. The diaphragm as shown in Figure 4 is micromachined using anisotropic wet-etching, where the etch rate is dependent on the crystal direction. We therefore get sidewalls with a characteristic slope of 54.7 degrees. By using other micromachining technologies like deep reactive ion etching (DRIE) it is also possible to get sidewalls with a 90 degree angle like shown for the support die in Figure 2.

2.1.2 Electrical properties of silicon

A semiconductor like silicon has an electrical conductivity between insulators and metals. The electrical conductivity can be altered by adding small quantities of impurity ions from neighboring elements in the periodic system. This is called *doping*, and it can be done by a number of established semiconductor processes like diffusion and ion implantation. After doping, silicon can be either n-type or p-type. N-type means that there is surplus of negatively charged electrons and p-type means that there is a surplus of positively charged holes.

2.1.3 The silicon piezoresistor

A simple form of a silicon piezoresistor can be realized by creating diffused piezoresistors in a silicon substrate. The resistors are defined by localized doping of the silicon substrate followed by a high temperature process. This will result in resistor geometries with unique electrical properties depending on the type and amount of impurities introduced.

The individual resistors are electrically connected to form a complete circuit using patterned thin film metallization on top of an insulating oxide. Figure 5 shows an example of a diffused p-type piezoresistor geometry in a n-type silicon substrate. The effective resistance is defined by the actual geometry, the semiconductor doping profile and doping levels, and the resistor is isolated from the substrate by a reverse biased pn-junction. Ohmic contact between metal and the p-type resistor is made by p+ diffusion (where p+ means *heavily* doped p type) in the contact areas, and the top surface is protected by a silicon dioxide insulating layer.

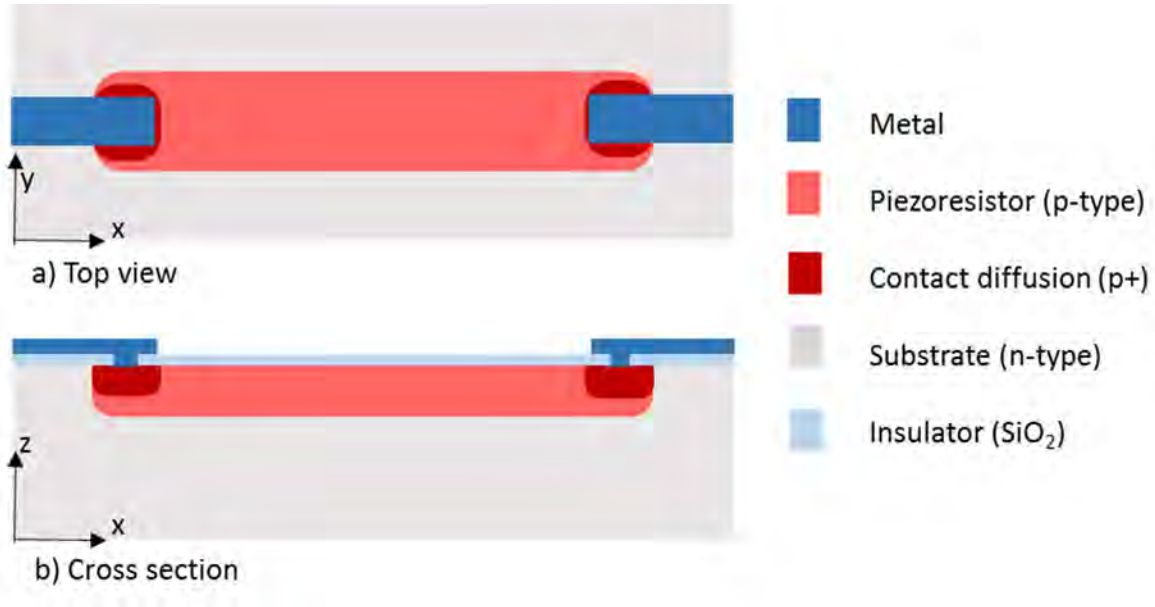

Figure 5 Piezoresistor layout

For a homogenous block of material of length *l* and cross section area *A*, the electrical resistance *R* between the end points can be expressed as

$$R = \frac{\rho l}{A} \tag{1}$$

where ρ is the electrical resistivity of the material. For many materials, ρ can be considered constant as a function of applied mechanical stress, and the resulting resistance change due to mechanical strain is mostly due to a change of geometry affecting the length and cross section area.

In a piezoresistor, the resistivity will change with mechanical stress [5] due to changes of the mobilities of electrons and holes. This effect, called the *piezoresistive effect*, is highly dependent on the crystallographic directions of the semiconductor as well as the applied stress directions, resulting in a rather complex tensor-notation. Further details can be found in Ref. [1].

For a p-type piezoresistor aligned with the silicon <110> directions, the resistance change due to a uniform mechanical stress can be expressed as

$$\frac{\Delta \mathrm{R}}{\mathrm{R}} = \pi_{\mathrm{l}}\sigma_{\mathrm{l}} + \pi_{\mathrm{t}}\sigma_{\mathrm{t}} \tag{2}$$

where σ_l is the mechanical stress parallel to the current flow (longitudinal) and σ_t is the mechanical stress perpendicular to the current flow (transversal) in the piezoresistor. π_l and π_t are the longitudinal and transversal piezoresistive coefficients. The longitudinal and transversal piezoresistive coefficients, π_l and π_t, can be expressed as

$$\pi_l = \frac{1}{2}(\pi_{11} + \pi_{12} + \pi_{44}) \tag{3}$$

$$\pi_t = \frac{1}{2}(\pi_{11} + \pi_{12} - \pi_{44}) \tag{4}$$

where π_{11}, π_{12} and π_{44} are components of the piezoresistive tensor.

In 1954, Smith [5] fully characterized the piezoresistive coefficient for lightly doped (10^{16} cm^{-3}) bars of silicon. He found π_{11} = 6.6 x 10^{-11} Pa^{-1}, π_{12} = -1.1 x 10^{-11} Pa^{-1} and π_{44} = 138.1 x 10^{-11} Pa^{-1} for the piezoresistance in the <110> crystallographic directions on the (100) plane of p-type silicon. Later, scientists have reported values for other doping

levels and by using diffused resistors, as well as characterizing the coefficients versus temperature [1], but the experimental data from Ref. [5] is still generally used for most introductory examples found in literature.

Based on typically reported values for the piezoresistive coefficients [5], we can use that $\pi_l \approx -\pi_t$, and (2) can then be expressed in the locally aligned coordinate system as

$$\frac{\Delta R}{R} = \frac{\pi_{44}}{2}(\sigma_x - \sigma_y) \tag{5}$$

where σ_x is x-axis normal stress and σ_y is the y-axis normal stress in the local coordinate system. Stress induced resistance change for a p-type piezoresistor is thus proportional to the *differential stress* (σ_x - σ_y) at the piezoresistor positions.

Typical values for the SP82 type of sensor die shows a full scale resistance change ΔR of 100 Ω at a pressure of 100 kPa. This corresponds to 0.1 Ω/hPa.

Piezoresistors are also highly temperature dependent, with a temperature coefficient of resistivity (TCR) in the order of 2200 ppm/°C. For the nominal 5 kΩ piezoresistors in SP82, this corresponds to 11 Ω/°C. For measuring a pressure difference of 0.1 hPa, we thus have to detect a resistance changes of 0.01 Ω on a signal that varies with 11 Ω/°C as a function of temperature. To be able to do this, we need to compensate for the temperature related variation.

2.1.4 Mechanical stress in a square diaphragm

When a pressure is applied from the bottom side of the silicon diaphragm in Figure 4, the diaphragm will bulge slightly upwards. With the geometry as shown in Figure 4 and a pressure of 100 kPa (1 bar), the maximum displacement at the center of the diaphragm will be less than 4 µm, with zero displacement at the diaphragm edges. For piezoresistors, it is not the displacement that is important, but the difference between mechanical stress in two directions. Figure 6 shows calculated x-axis normal stress (σ_x) and y-axis normal stress (σ_y) for the top surface of the geometry in Figure 4 with an applied test pressure of 100 kPa. At the edges of the diaphragm there is a high

compressive stress (negative values) and there is also a high tensile (positive values) stress towards the center of the diaphragm.

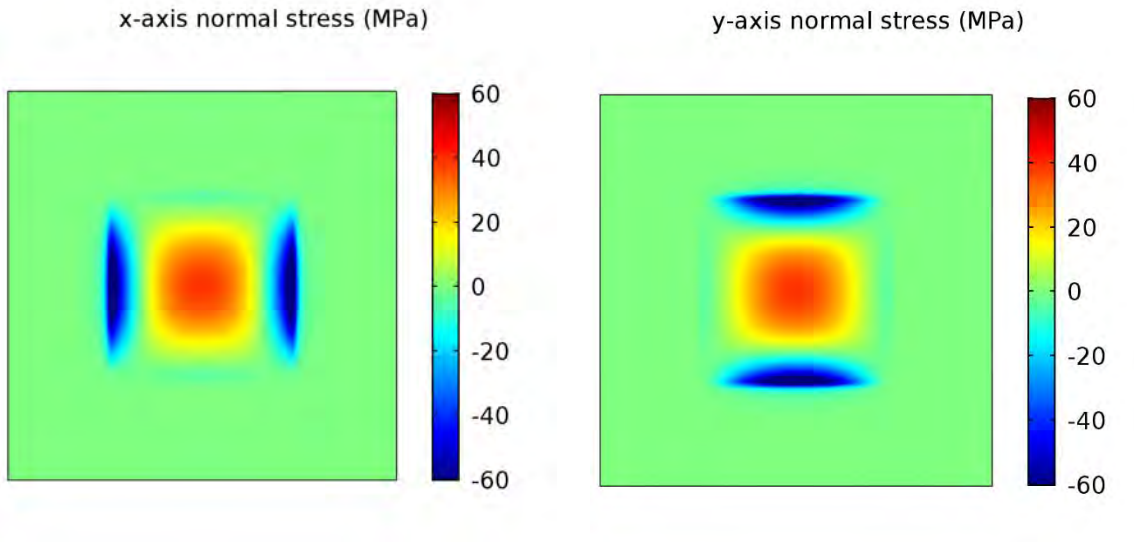

Figure 6 Left: x-axis normal stress (σ_x) and Right: y-axis normal stress (σ_y) - on the top surface of the sensor diaphragm die with an applied pressure from bottom of 100 kPa

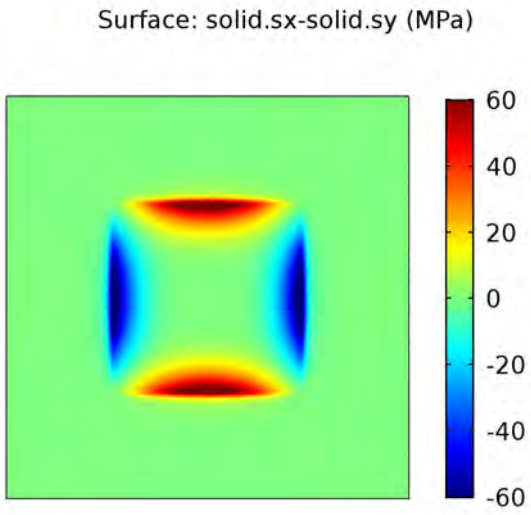

Figure 7 Differential stress ($\sigma_x - \sigma_y$) on top surface of sensor diaphragm die with an applied pressure from bottom of 100 kPa

Figure 7 shows the calculated differential stress ($\sigma_x - \sigma_y$) on the surface. Notice that the differential stress is zero at the center and maximum at the mid-point of the

diaphragm edges. Also note that the sign is positive along two of the edges and negative along the two other edges.

Using the piezoresistor positions from Figure 4 and inserting the differential stress results from the square membrane of Figure 7 into (5) will result in two resistors with increasing and two resistors with decreasing resistance with pressure.

2.1.5 The Wheatstone bridge

A common way of connecting four piezoresistors is the closed Wheatstone bridge configuration as shown in Figure 8. This configuration converts the resistance change into an output signal voltage.

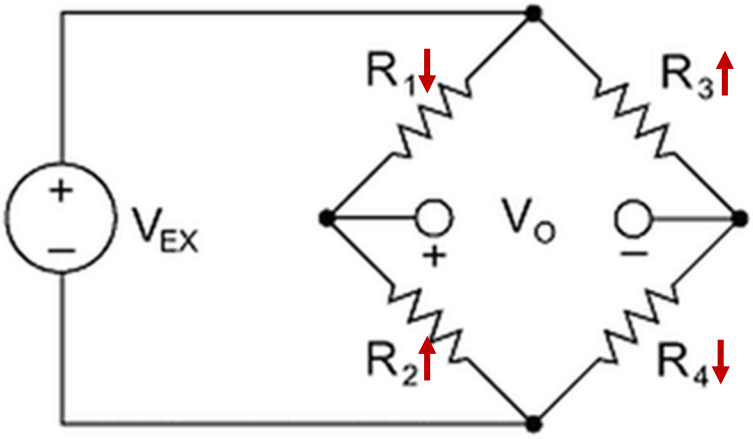

Figure 8 Typical constant voltage Wheatstone full-bridge configuration (red arrows indicate resistance change with increasing pressure)

The output signal V_O can be expressed as

$$\frac{V_O}{V_{EX}} = \frac{R_2}{R_1 + R_2} - \frac{R_4}{R_3 + R_4} \tag{6}$$

where V_{EX} is the excitation voltage and R_1 to R_4 is the resistance of the pressure sensing piezoresistors. For this configuration, all four resistors will contribute to the resulting signal if R_1 and R_4 decrease and R_2 and R_3 increase as function of pressure.

Ignoring higher order contributions to TCR, the resistance of the individual piezoresistors R_i (where i = 1..4) can be simplified as

$$R_i = R_{0,i}(1 + \alpha_i \, \Delta T + \frac{\pi_{44}}{2}(\sigma_{\mathrm{x,i}} - \sigma_{\mathrm{y,i}})) \tag{7}$$

where $R_{0,i}$ is the resistance at a reference temperature, α_i is the temperature coefficient of resistance (TCR) for the individual resistors, ΔT is the temperature change and $(\sigma_{\mathrm{x,i}} - \sigma_{\mathrm{y,i}})$ is the differential stress at the piezoresistor position.

If the four piezoresistors in (6) share a common nominal resistance R_0 and TCR (α), the output signal change due to temperature is effectively cancelled. However, due to small variations in doping levels and geometry in practical implementations, there will be small differences between the individual resistors that need to be compensated for high-accuracy applications. Temperature dependent residual stress from manufacturing will also give stress-dependent contribution from the stress-sensitive part of (7), even when external pressure is not applied.

Replacing the voltage source V_{EX} in Figure 8 with a constant current source I_{EX}, will result in an increasing excitation voltage versus temperature. This can be used as an initial compensation of the negative temperature coefficient resulting from the positive TCR.

2.2 Basic properties

An assembled pressure sensor is usually characterized using a fixed excitation voltage (or current) at specified environmental conditions through its:

- **Zero-point offset** Output signal at zero pressure (mV). (Often normalized to the excitation as mV/V for constant voltage excitation or mV/mA for constant current excitation)
- **Full Scale (FS)** Output signal at rated maximum pressure (mV)
- **Sensitivity** Output signal per unit pressure change (for example mV/bar)

- **Non-Linearity** Maximum deviation of output signal versus pressure from linear behavior (% FS)
- **Repeatability** A measure of how repeatable the measurements are for the same input pressure during pressure cycling (% FS)

It is normal to also specify some temperature related effects:

- **TCO** Temperature coefficient of zero-point offset. Can be approximated as a linear change for a limited temperature span (μV/°C or %FS/°C), or a more detailed behavior can be presented using a graph of zero-point versus temperature.
- **TCS** Temperature coefficient of sensitivity. Can be approximated as a linear change for a limited temperature span (%FS/°C), or a more detailed behavior can be presented using a graph of full-scale signal versus temperature.

2.2.1 Long-term drift

A signal *drift* is a continuous signal change over time, while a signal *shift* is a sudden change of the signal at a specific time. Long-term drift (or long-term stability) is a measure of how the sensor output signal will change over a long time period, for example a year. It will often contain both drift and shift-related signal changes, as it is difficult to distinguish one from the other without continuous monitoring of the signal. Long-term drift is typically specified as %FS/year or ppm of FS/year. This type of signal change may be caused by a variety of sources and cannot be easily compensated. A detailed study is needed to identify the materials and properties causing this effect, and to minimize these.

If the source of the drift is known, the test-time for testing of long-term stability can be reduced by performing accelerated testing. The drift is then typically accelerated by an elevated temperature or by thermal cycling.

2.2.2 Thermal hysteresis

Thermal hysteresis is the difference observed on the sensor output signal when subjected to an increasing versus decreasing temperature gradient. It can be caused by time dependent stress changes in the sensor structure, and is often omitted in the sensor specifications. Figure 9 shows an example of the output-signal deviation from reference pressure versus temperature for a calibrated sensor module, where the thermal hysteresis is represented by the *eye-opening* in the plot. The cloud of points includes deviation results for the whole pressure range obtained during a slowly increasing and decreasing temperature with a rate of change of only 0.2 °C/min. The complete temperature cycle takes approximately 24 hours, minimizing influence from short-term viscoelastic effects.

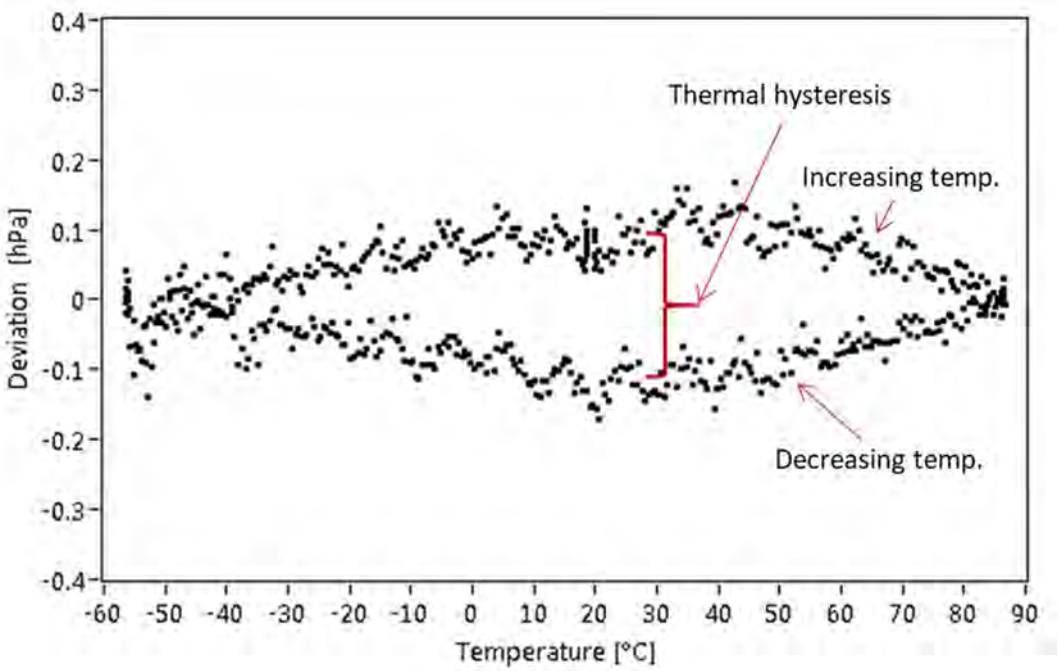

Figure 9 Example of thermal hysteresis for a calibrated sensor module

Compensation of thermal hysteresis effects is not trivial and would require continuous recording and storage of the sensor temperature and output signal. A better approach is therefore to search for the root causes and try to minimize these.

2.2.3 Total error band

For a calibrated sensor module, the total error band consists of the sum of contributions from the basic properties as well as thermal hysteresis during calibration. Using modern digital compensation technologies, most of the contributions from the basic properties can be compensated and the thermal hysteresis will often be the limiting factor.

3 Stability of piezoresistive pressure sensors

3.1 Introduction

There are a number of factors that might influence the stability of piezoresistive pressure sensors. These can be divided into electrical, mechanical and leakage related phenomena. Each of these will be covered in some details in the following sections, with references to relevant literature. The focus has not been to cover all details of each mechanism, but to give an overview of possible contributing phenomena. Environmental conditions like temperature and humidity have the potential to influence on both electrical as well as mechanical and leakage related drift mechanisms, and will be mentioned where appropriate.

3.2 Electrical drift mechanisms

3.2.1 Introduction

To better understand some of the possible electrical drift mechanisms for a piezoresistor, it might be useful to introduce some concepts from semiconductor physics. For the interested reader, there are a vast amount of literature available, such as Ref. [6, 7].

The layered structure of a metal conductor on an oxide-isolated silicon substrate resembles a Metal Oxide Semiconductor (MOS) capacitor where the charge on the metal is mirrored by a distributed charge in the silicon surface area. Dependent on the charge polarity and quantity on the metal as well as the doping type and levels of the silicon, the silicon surface can be driven into *accumulation*, *depletion* or *inversion*.

For n-type silicon, applying a small positive voltage between the metal and the silicon will result in an electrical field driving the mobile electrons in the silicon to a thin *accumulation* layer at the oxide-silicon interface.

If the applied voltage is reversed, the electrical field is also reversed, and the mobile electrons in the n-type silicon will be pushed away from the oxide-silicon interface. When the electrons are pushed away, a positive *space charge region* (*scr*) is created at the silicon-oxide interface consisting of the fixed donor atoms in the n-type silicon. Since the *scr* is depleted for majority carriers, it is often referred to as a *depletion region*. Further increasing the negative voltage will increase the depletion region width (W_d) until a maximum is reached and the surface layer near the oxide *inverts* its conduction type from n-type to p-type. This occurs at the *threshold voltage* (V_T). Figure 10 illustrates the charge distribution for an ideal MOS capacitor biased into inversion, together with the electrical field distribution. The equivalent MOS capacitor consists of two capacitors in series and performing C-V measurements on this structure can give valuable information of the amount and type of charge in the silicon dioxide.

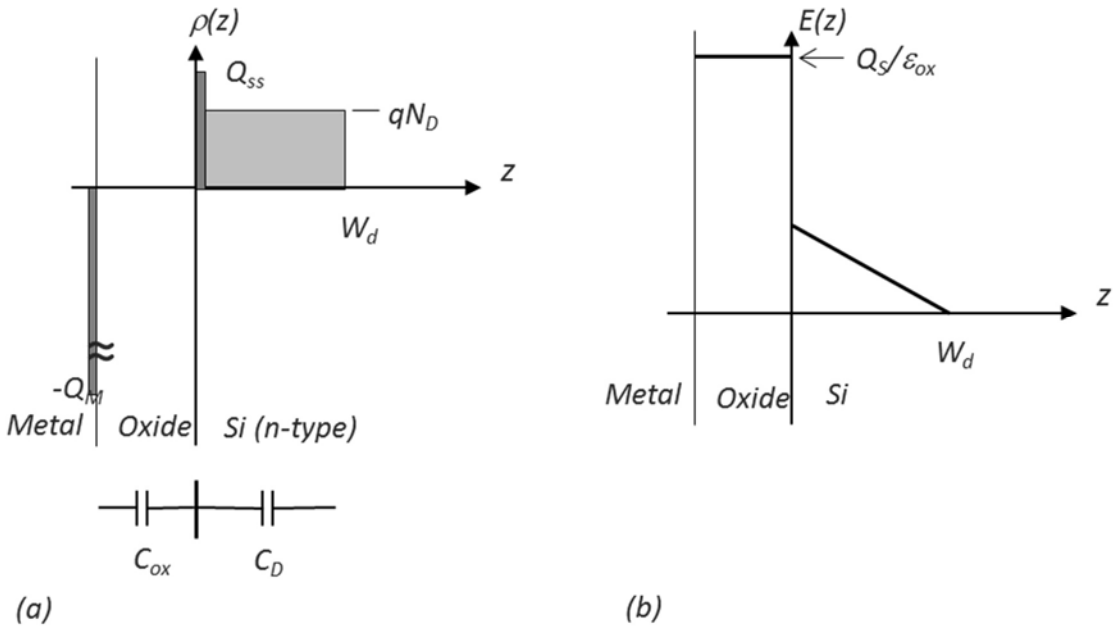

Figure 10 (a) Charge and equivalent capacitance (b) electrical field distribution in ideal MOS capacitor biased into inversion.

The *flat-band voltage* (V_{FB}) is the applied voltage resulting in zero *scr*. For the ideal case with no additional oxide charges we have

$$V_{\mathrm{FB}} = \phi_{\mathrm{ms}} \tag{8}$$

where ϕ_{ms} is the metal-semiconductor work function difference. However, a real oxide-semiconductor will have charges both within the oxide itself and at the oxide-semiconductor interface (elaborated in section 3.2.3). An expression of V_{FB} including the influence of these oxide charges is given by

$$V_{\mathrm{FB}} = \phi_{\mathrm{ms}} - \frac{Q'_{\mathrm{ss}}}{C_{\mathrm{ox}}} - \frac{1}{C_{\mathrm{ox}}}\int_0^{x_{ox}} \frac{x}{x_{\mathrm{ox}}}\rho(x)dx \tag{9}$$

where Q'_{ss} is the charge per unit area from surface states at the oxide-silicon interface, C_{ox} is the oxide capacitance, x_{ox} is the oxide thickness and $\rho(x)$ is a distribution function of charge. The second term of (9) is the influence from surface states at the oxide-silicon interface, while the third term describes the influence from a distributed charge across the thickness of the oxide with a given distribution function $\rho(x)$.

The *threshold voltage* (V_T) of the MOS configuration is the voltage at the metal that is needed for surface inversion and formation of a conductive channel at the semiconductor surface. It is expressed as

$$V_{\mathrm{T}} = V_{\mathrm{FB}} + V_{\mathrm{C}} - 2|\phi_{\mathrm{n}}| - \frac{1}{C_{\mathrm{ox}}}\sqrt{2\varepsilon_{\mathrm{Si}}qN_{\mathrm{D}}(2|\phi_{\mathrm{n}}| + V_{\mathrm{B}} - V_{\mathrm{C}})} \tag{10}$$

where V_{C} is the channel voltage, ϕ_{n} is the surface potential of the n-type silicon, $\varepsilon_{\mathrm{Si}}$ is the dielectric constant of silicon, q is the elementary charge, N_{D} is the donor-density and V_{B} is the bulk (or substrate) voltage.

Formation of conducting channels at the silicon surface will influence the current distribution in a sensor design, thus influencing the output signal. The geometry of a surface piezoresistor is also directly influenced by the width of its surrounding depletion zones, and is thus influenced by the depletion zone near the silicon surface. Since the surface depletion width is strongly dependent on charge in and on the oxide, possible charge redistribution should be avoided for obtaining a stable design.

3.2.2 Drift due to charges on the passivation surface

Already in 1959, Atalla *et al.* [8] studied instability phenomena in passivated pn-junctions under high humidity conditions. This was followed up by Shockley *et al.* [9], and it was concluded that observed channel formations and changes of device characteristics was caused by ion motion on the oxide layer. The ion motion was caused by the fringing field of the junction and strongly accelerated by humidity.

Another source of surface charges is charging from the electrical potential of nearby surface metal [10]. This effect is influenced by the oxide surface-conductivity and is also strongly accelerated by humidity and temperature.

Ho *et al.* [11] characterized the dynamic charging and discharging curves by measuring the current between two deposited electrodes on the oxide surface. Schlegel *et al.* [12] described a useful test structure for characterization of surface ion behavior and demonstrated the effects of time, humidity, temperature, voltage as well as previous testing history on the behavior. The observations were made by observing the electrical resistance between two diffused junctions, where accumulation of surface charge resulted in inversion of the underlying silicon. Martin *et al.* [13] used the Kelvin option of an atomic force microscopy (AFM) to deposit and then measure charge distribution versus time on silicon dioxide. They also found a strong dependence of the charge decay time constants on humidity.

These effects can be reduced by covering the oxide by a metal to keep the top surface of the oxide to a fixed electrical potential, or by adding distance to the charge by using a thicker oxide layer or a protective gel [14]. It is also important to limit the amount of ionic contamination to a minimum and hermetically encapsulate the device in a dry atmosphere. Voorthuyzen *et al.* [15] found that chemical modification of the oxide surface by using silanizing agents like HMDS (hexamethyldisilazane), strongly reduced the adsorption of water on the surface thus reducing the surface conductivity.

Park *et al.* [14] studied offset drift due to surface charge for a piezoresistive pressure sensor. They used a varying substrate bias to control parasitic FET formation and estimate the amount of surface charge.

Sager *et al.* [16, 17] studied the influence of humidity as a failure source in piezoresistive sensors. They found that the formation of condensed water on the sensor surface caused changes to the sensor offset voltage, caused by complex physical and chemical mechanisms. The effects are summarized in Figure 11 where (A) to (C) illustrates influence on the current flow in the piezoresistor area, while (D) to (F) shows the effect of charges at and in the passivation layers.

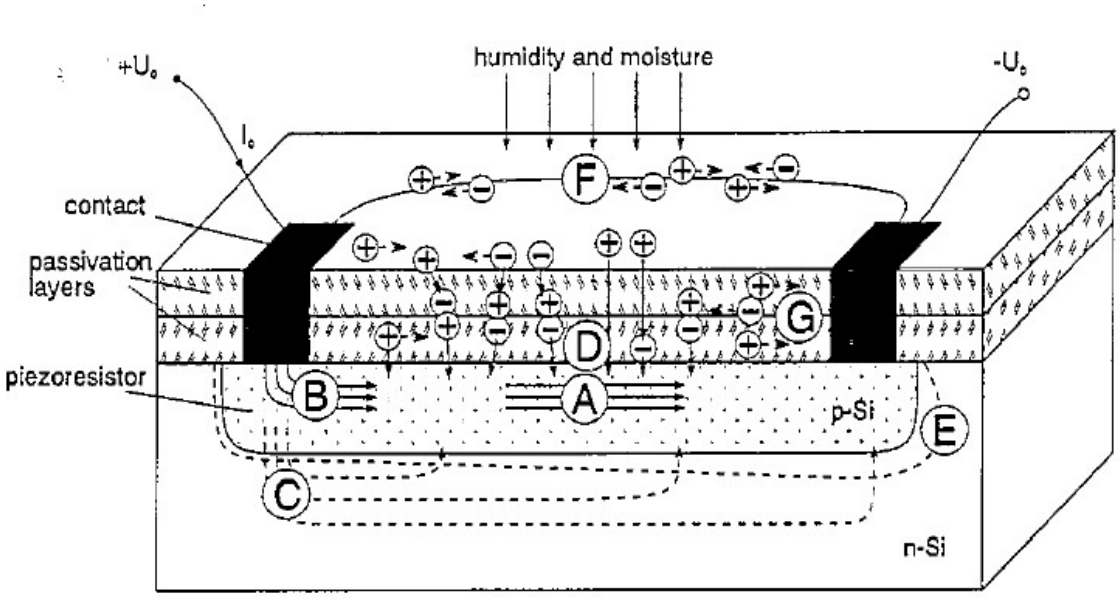

Figure 11 Humidity influence coupled with semiconductor charge effects on planar resistors. **The influences on the current-flow mechanism in the piezoresistor area:** (A) current flow through the piezoresistor; (B) changes of contact resistance between the metal and the semiconductor; (C) current-flow caused by incomplete insulation of the p-n junctions. **Charges at and in the passivation layers:** (D) changes of the conductivity at the upper side of the resistor; (E) changes of the p-n behavior at the border of the resistor (changes of the reverse current, channel formation and breakdowns); (F) current flow at the surface of the passivation layers; (G) current flow in the volume of passivation layers. (From [16]. Reprinted with permission)

3.2.3 Drift due to charges in the passivation

During the development of planar MOSFET structures during the 1960's, charge migration in the oxide was found to be a limiting factor [18]. There are generally four types of charges that should be considered (ref Figure 12): interface-trapped charges (Q_{it}), fixed oxide charge (Q_f), oxide-trapped charge (Q_{ot}) and mobile ionic charge (Q_m).

Any contamination of silicon dioxide with alkali ions such as sodium or potassium during manufacturing and handling may result in instabilities both due to charge redistribution on the surface as well as in the silicon dioxide under the influence of electrical fields.

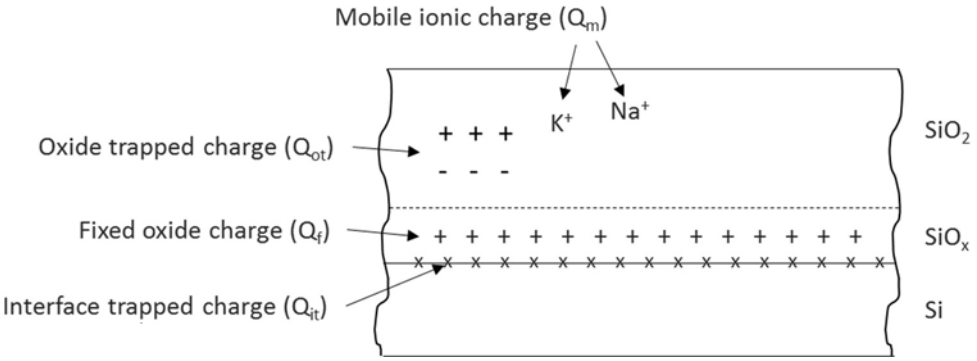

Figure 12 Charges in a silicon dioxide on silicon layer

Another source of charging is ionizing radiation [10]. Holbert *et al.* [19] investigated the radiation hardness of piezoresistive MEMS devices and found that when radiated with gamma rays, the volume for current flow through the resistors were reduced. This was attributed to the formation of oxide-trapped and interface-trapped charges, generating a depletion zone at the silicon surface effectively reducing the thickness of the piezoresistors.

3.2.4 Parasitic FET

If we consider the two terminals of a piezoresistor as the source and drain in a gateless MOSFET, and add a charge on the oxide surface between them, a high surface charge

might result in a channel formation between the two terminals, effectively reducing the current that flows through the piezoresistor. This is called a *parasitic FET*.

The threshold voltage for channel formation (10) will be dependent on the doping level of the bulk silicon (or epitaxial layer for a buried resistor), electrical potentials of the substrate and resistor terminals, the amount of mobile charges in the oxide, surface charges and the oxide thickness.

In a study of parasitic MOS formation mechanism in plastic encapsulated MOS devices [20], it was found that also ions from nearby plastic encapsulation can contribute to the formation of a parasitic FET.

3.2.5 Buried resistors

A successful approach for removing charge related effects on/in the passivation has been to use *buried resistors* [21-23]. This is also used for the SP82 piezoresistor design, where the piezoresistors are covered by an epitaxial grown n^+ type silicon as illustrated in Figure 13.

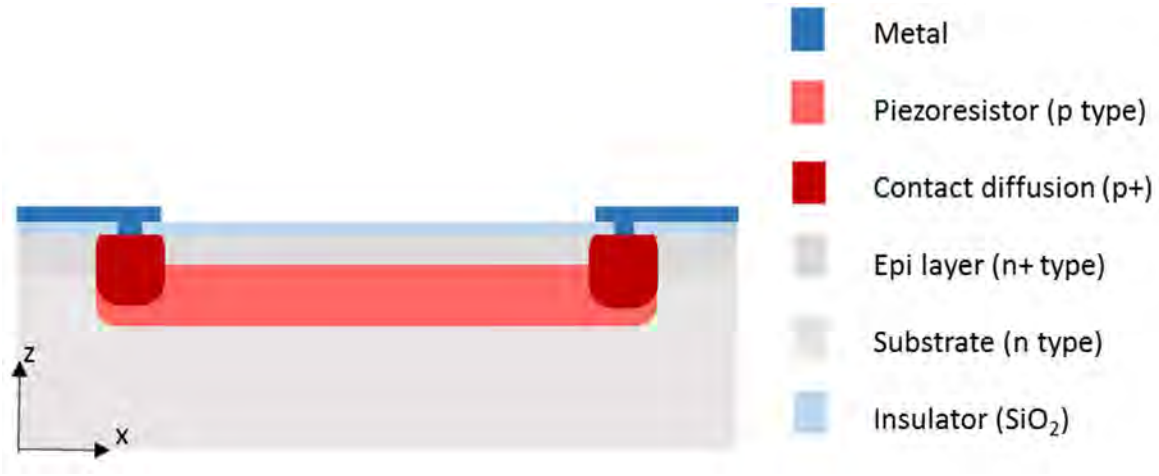

Figure 13 Buried p-type piezoresistor in a n-type silicon substrate

After manufacturing surface resistors, a thin epitaxial layer of n^+ type silicon is grown on the top surface of the wafer. Contact diffusion is done through the epi layer to the p-type piezoresistor. By careful design of the epi-layer thickness and doping

concentration, the piezoresistor is effectively shielded from influence of surface charge. For a buried resistor, the effect of charge on/in the passivation will change the charge distribution at the top of the epi-layer, but with sufficient thickness and doping levels, the charge distribution in the piezoresistor is unaffected. Due to the increased pn-junction area, the resulting leak current is slightly increased. The sensitivity is also slightly reduced due to the shorter distance to the stress-neutral plane in a diaphragm.

Some simulation results of resistors with a shield layer have been reported in [24].

3.2.6 Leak current in reverse biased pn junctions

Diffused piezoresistors are isolated by reverse biased pn junctions. The reverse bias will result in a highly temperature dependent reverse current, often called leakage current. This will limit the high temperature range to approximately 125 to 150 °C for practical applications. There are three major contributions to the leakage current: diffusion current (I_D), bulk generation current (I_G) and surface generation current ($I_{G,\text{surface states}}$) [25]. The total leakage current (I_{leak}) can be expressed as

$$I_{\text{leak}} = I_{\text{D}} + I_{\text{G}} + I_{\text{G,surface states}} \tag{11}$$

The diffusion current (I_{D}) can be subdivided into contributions from the substrate and from the resistor volume (plus from the epi-region for the buried resistor in 3.2.5)

The bulk generation current (I_{G}) can be subdivided into contributions from the p+/substrate *scr* and from the surface depletion *scr* (plus from the p+/epi-region for the buried resistor in 3.2.5)

The surface generation current ($I_{\text{G,surface dstates}}$) is surface generation current in surface *scr* from surface states. These surface states origins from the abrupt termination of the periodic silicon crystal structure caused by wafer cutting and surface treatment.

When configured in a Wheatstone bridge, the electrical potential between the substrate and the piezoresistors (and thus the depletion region widths and threshold

voltage) will vary along the length of the resistors resulting in different contributions to leakage current from the upper and lower part of the bridge.

Sun *et al.* [26] modelled the reverse current and its effects on the thermal drift of the offset voltage for piezoresistive pressure sensors. They found that both the reverse current as well as differences in TCR between the four piezoresistors had a great influence on the thermal drift of the output voltage, especially for temperatures above ~50 °C

3.2.7 Substrate bias effect

For a design with p-type piezoresistors on a n-type substrate, the substrate potential should be maintained at the highest potential used during operation to maintain a low leak current and proper isolation between the circuit elements.

The reverse bias will influence the *scr* width of the reverse biased pn-junction and modulate the physical size of the piezoresistor [6]. As the reverse bias is increased, the effective dimensions of the piezoresistor will decrease and the resulting resistance will increase. As mentioned in section 3.2.6, an increase of the *scr* will also result in an increased leak current. For stability, the reverse bias should therefore be kept at well-defined levels.

3.2.8 Electrostatic forces

Separation of charge will result in an electrostatic force possibly influencing the mechanical stress at the piezoresistor positions. It should therefore be considered as a possible drift-mechanism.

Electrostatic potentials between the reference die surface and the sensor diaphragm surface is one possibility, but there will also be electrostatic forces at other locations, such as across the silicon oxide layer and across the depletion regions in the semiconductor.

Is it possible that the electrostatic force between separated charges in a piezoresistor design can result in stress changes that are detectable on the sensor output signal?

The electrostatic force from charging of a dielectric surface has been identified as a root cause for tilting angle drift in MEMS micromirrors [27], where the charge distribution is a function of the surface resistance of the dielectric film. Bouwstra *et al.* [28] used the electrostatic force in a dielectric layer between two electrodes to mechanically excite a vibrating cantilever. Ransley *et al.* [29] has demonstrated that the electrostatic force across the depletion layer of a pn-junction can be used for designing an actuator.

3.2.9 Drift in the series resistance of the interconnect

The series resistance consists of the sum of the resistance of the doped interconnect, the contact diffusion, contact resistance between the diffusion and metal, the metal interconnect line, the wire bond and the contact resistance between the wirebond and wire at both ends. Any change of this series resistance might affect the sensor output signal. If the piezoresistors are configured in a perfectly symmetric Wheatstone bridge, small distributed variations in the interconnect resistance will be cancelled with a neglectable influence on the sensor zero point. It is therefore important to have a symmetric metallization design with equal length and contact hole areas to minimize the effect of possible drift in the series resistance on the sensor output signal.

Andrei *et al.* [30] found that extended exposure at 150 °C caused a systematic decrease of AlTi/TiW metal-line resistance as well as a significant contact-resistance increase. Lloyd *et al.* [31] found a resistance decay in Al thin-film conductors after high current density stressing, where the decay rate was suggested to origin from mechanical stress relaxation.

The growth of Au-Al intermetallic compounds at wirebond interfaces has been studied by several authors [32-34] due to the possibility of reliability issues. Zin *et al.* [34] found that electromigration could also result in wirebond failure related to an increased growth of Au-Al intermetallic compounds. The failure rate was found to be much faster for electron flow from Au to Al than in the opposite direction. Prior to complete failure, the contact resistance increased and became unstable.

3.3 Mechanical drift mechanisms

3.3.1 Mechanical stress in thin-film metal and surface materials

As opposed to single-crystal silicon, mechanical stress in thin-film aluminum used for the interconnect may contain large plastic, visco-plastic and visco-elastic effects [35-40]. The large difference in coefficient of thermal expansion (CTE) between the silicon and the deposited metal will result in significant time-dependent thermo-mechanical stress.

The effect on the output signal can be reduced by a careful geometric design minimizing the amount of metal and maximizing the distance between the piezoresistors and the metal [41]. The distance from the stress sensitive piezoresistors to metal can also be increased by using highly doped silicon as buried leads [42]. In Article V, we describe an approach for in situ observation of metal properties in a piezoresistive pressure sensor.

Thermally grown silicon dioxide is often used for passivation of the silicon die surface. Blech *et al.* [43] studied the effects of humidity on the mechanical stress in 1 µm thick silicon dioxide films. They found no influence on thermally grown silicon oxide, but for chemical vapor deposited (CVD) silicon dioxide they found a clear influence from humidity. The stress in CVD films increased when exposed to dry ambient, and thermal cycling showed a clear hysteresis effect. This was attributed to the open and porous structure and absorption and desorption of water. The use of CVD silicon dioxide (or other porous materials) should therefore be omitted in order to minimize humidity influence on the residual stress.

Aluminum will form a thin layer (approximately 5 nm) of aluminum oxide (Al_2O_3) when exposed to air at room temperature. With a high molar volume, it offers a natural sealant against further influence from the environment and thus contributes to the corrosion resistance of aluminum. However, the mechanical properties of aluminum oxide differ from aluminum. Saif *et al.* [44] studied the effect from native aluminum

oxide on the elastic response of thin aluminum films. They found a much lower influence than expected, which were attributed to the surface roughness resulting in a wavy structure of the native oxide layer.

3.3.2 Stress changes in a bonded die-stack

The physical bonding of the various dies constituting the inner part of a MEMS pressure sensor will introduce mechanical stress in the structure. Any changes in this stress might affect the sensor output-signal.

As long as this stress is constant or shows a repeatable and perfect elastic change over temperature and applied pressure, it will contribute to the observed sensor behavior, and can be removed at subsequent characterization and correction steps.

Three common die bonding technologies are glass-frit bonding, anodic bonding and direct wafer bonding. As they all contain brittle materials at the bonding interface, an important stress relaxation mechanism to consider is the possibility of microcrack formation.

3.3.2.1 Glass frit bonding

Glass frit bonding is based on a low melting point seal glass material as the intermediate bonding layer. The seal glass is normally purchased as a viscous glass frit paste, where the various glass forming components have been milled into a powder with small grain sizes and mixed with an inorganic filler, organic binder and solvents to form a printable glass paste. After deposition, normally done by a screen printing technology, a drying process is performed to drive out organic components and form a coherent patterned glass layer. The actual sealing process is done by aligning the die (or wafer) containing the seal glass with a second die (or wafer) and then applying a small force at an elevated temperature of approximately 400-450°C for a given time. The resulting bonding layer consist of a thin glass layer of approximately 10 to 20 µm [45]. One of the main advantages of glass frit bonding is the possibility to bond rough processed surfaces. A scanning electron microscope image of a cross section of a

bonded glass layer is shown in Figure 14. As seen, the glass consists of a glass matrix modified by larger filler particles. The filler particles (often made of the mineral cordierite) are used to adapt the coefficient of thermal expansion of the bond to the materials being bonded.

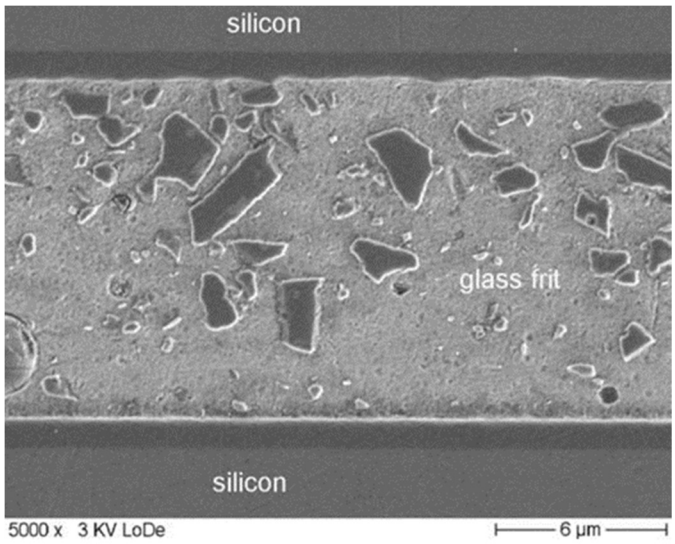

Figure 14 Cross section (SEM) of a bonded glass frit layer (From[45]. Reprinted with permission)

Glass frit is a brittle material where fracture is mainly experienced under tensile stress combined with small defects in the material. Having a typical glass transition temperature of 330 °C and a CTE of 6 ppm/K, cooling a silicon/glass-frit laminate to 20 °C will result in a biaxial stress of the order of 89 to 147 MPa depending on the exact material characteristics. Variations in the amount and distribution of the glass frit material can also results in regions of even higher mechanical stress, as discussed in Article I and Article III. These regions will be more prone to stress relaxation through the development of microcracks. Several studies have been performed on the mechanical properties, reliability and crack growth mechanisms in glass frit bonded samples [45-48]. Sub-critical crack growth (described in section 3.3.2.4) will alter the stress distribution and might be detectable as signal-drift in a stress sensitive pressure sensor.

As shown in Figure 14, glass frit is not a homogenous material, and large mechanical stress between the various components might cause local stress relaxation through the development of microcracks. Petzold *et al.* [46] observed that significant crack branching could occur at the crack tip of long-term loaded (3 months) glass-frit laminates during crack growth measurements. This was attributed to the filler particles and the adhesion between filler and glass-matrix.

Several authors have reported on the possibility of lead precipitation at the silicon-glass interface. [49-52]. Glien [49] described the lead precipitation as a metallic lead forming redox reaction at the bonding interface to silicon during high bonding temperatures. The main reaction is:

$$2\ PbO + Si \rightarrow 2\ Pb + SiO_2 \qquad (12)$$

Boettge *et al.* [50] studied the interface reactions between silicon and glass frit material and found that lead precipitation formed at the interface reduce the tensile strength of the bonding interface, forming a risk for both bonding quality and reliability. The precipitates can act as initial defects and stress concentrators enhancing crack initiations.

The deposition of silicon oxide or metallic intermediate layers reduces the probability of lead precipitation, acting as a diffusion barrier. Annealing of the samples with lead precipitation in [50] showed that aging for 7 days at 400 °C could result in growth of the precipitate diameters from initially 0.15 µm to 1.43 µm. It was also found that the growth of the precipitations saturated at a size of approximately 1.2 µm.

Although the formation of lead precipitates is only found under certain combinations of processing conditions, this phenomenon should be kept in mind when adjusting process parameters. Metallic lead will have very different thermo-mechanical properties from the bulk glass frit material and this could result in change of stress distribution in the bonded devices.

3.3.2.2 Anodic bonding

Anodic bonding is a well-established bonding method for bonding silicon to glass structures or bonding of two silicon wafers using a thin intermediate glass film [53]. The bonding is performed at a relative low temperature (300 – 450 °C) and can thus be done on metallized structures. It requires the use of alkali-containing (typically Na^+ ions) glass that can be polarized when a high DC voltage is applied. When the Na^+ ions are displaced from the bonding interface, the electrical field across the depleted region results in a strong electrostatic force bringing two surfaces into intimate contact. This results in formation of a thin silicon dioxide bonding layer.

One possible disadvantage of anodic bonding is potential surface contamination caused by sodium (Na) from the glass. This will influence on electrical performance as discussed in Section 3.2. Foreign particles in the glass or other stress concentrations can also act as crack initiating points for the formation of microcracks at the interface. As discussed in Section 3.3.2.1, sub-critical crack growth might alter the stress distribution and might be detectable as signal-drift in a stress sensitive pressure sensor.

3.3.2.3 Direct Wafer Bonding (Fusion bonding)

Hydrophilic direct wafer bonding (DWB) or fusion bonding is a well-established process for joining silicon wafers [53]. Silicon On Insulator (SOI) is a typical application utilizing DWB.

The initial bond process starts at room temperature when two hydrophilic silicon wafers are brought into contact and the chemisorbed water molecules at opposing surfaces forms hydrogen bonds. The bond strength depends on the number of hydrogen bonds and therefore on the number of silanol groups (Si-OH) and water molecules. In order to control the propagation of the bond wave and to avoid voids caused by trapped gas, a mechanical fixture with spacers can be used for applying a small mechanical force firstly at the center of the wafers. A subsequent annealing is then performed to increase the bonding strength. The high annealing temperature

results in increased viscous flow of the materials which leads to greater surface contact between the wafers and increased bond strength. During annealing, the water molecules diffuse out along the interface or through the native oxide to the bulk silicon. Increasing temperatures results in opposing silanol groups reacting with each other forming strong covalent siloxane (Si-O-Si) bonds according to the following reaction:

$$\text{Si-OH} + \text{Si-OH} \rightarrow \text{Si-O-Si} + H_2O \tag{13}$$

Typical annealing temperatures used are > 800 °C, and hydrophilic direct wafer bonding is thus unsuitable for metallized structures. Thin geometries containing vacuum cavities might also be problematic if annealed under atmospheric pressure, due to plastic deformation at the high annealing temperatures.

3.3.2.4 Stress corrosion cracking

Central to the stability of bonded structures where glass is used as the bonding material is brittle fracture mechanics and the concept of *environmentally enhanced subcritical crack growth* or *stress-corrosion cracking* [54, 55]. Other terms used in the glass literature are *static fatigue* or *delayed failure* [56]. As both the glass-frit glass composition as well as the borosilicate glass normally used for anodic bonding contains a large proportion of silicon oxide, the mechanism of stress corrosion cracking is a probable source for stress relaxation also for these bonding processes.

The susceptibility of siloxane bonds (Si-O-Si) to stress corrosion effects has been extensively investigated for silica glasses (glass based on silicate or SiO_2), and an review of this can be found in [55].

The present theory for explaining the glass behavior in the stress-corrosion regime (often called *region I*) relies on water chemical attack of stressed siloxane bonds [54]. The applied stress will modify the siloxane bond by modifying the Si-O-Si bond angle such that the water molecule can be absorbed and the siloxane bond can be broken

into two silanol bonds as shown in Figure 15. This reaction is the reverse of (13) and can be written as

$$Si\text{-}O\text{-}Si + H_2O \rightarrow Si\text{-}OH + HO\text{-}Si \quad (14)$$

Since one water molecule is needed to break each siloxane bond, this reaction is accelerated by increasing level of humidity.

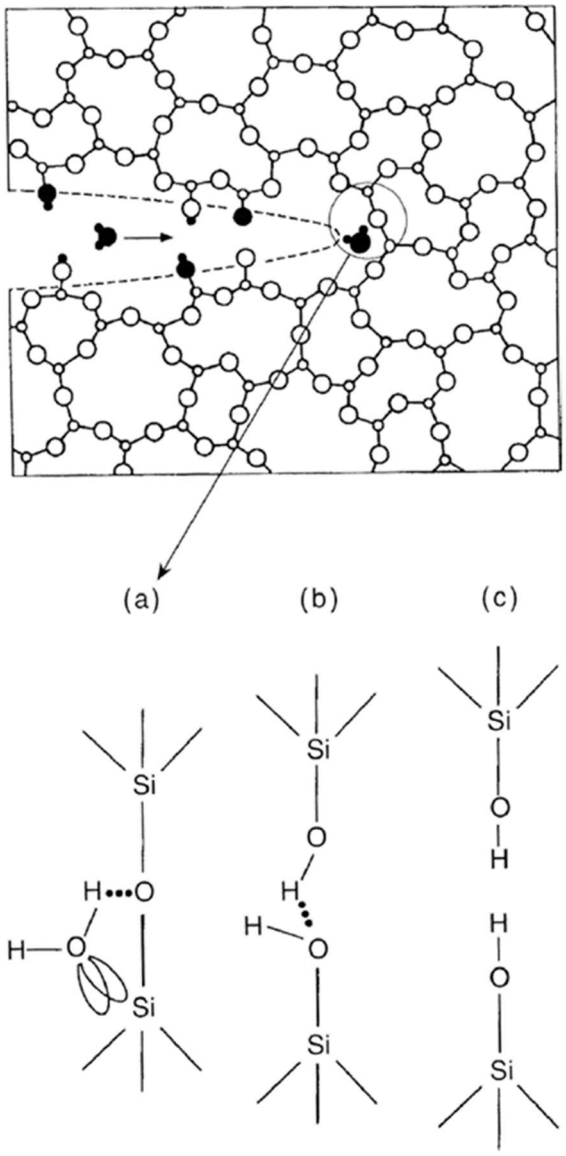

Figure 15 Basic process of stress-corrosion reaction (from [55]. © IOP Publishing. Reproduced with permission. All rights reserved)

Some glasses will exhibit a stress threshold behavior below which the fracture velocity falls to undetectable levels [55]. The kinetics of crack propagation is also strongly influenced by stress loading distribution [57] and material homogeneity.

Akisanya *et al.* [57] studied brittle fracture paths as function of mechanical loading mode mix for adhesive joints.

Bagdahn *et al.* [58] studied fatigue of hydrophilic direct wafer-bonded silicon under static and cyclic loading. They found that fatigue was related to the siloxane bonds in the bonded surface between the silicon wafers.

Masteika *et al.* [59] performed a series of tests on DWB wafers under various levels of relative humidity. They found that stress corrosion of DWB samples was similar to stress corrosion described for silica, and that the Wiederhorn equation (often used in stress corrosion studies of glass) could be used for modelling the crack propagation speed. This was further elaborated in a recent study by Fournel *et al.* [60], where also the role of trapped water during the bonding process was described.

Kern [61] studied the stability of glass frit bonding. An initial lowering of the critical energy release rate G_C when exposed to high humidity levels (85% RH at 85 °C for 1 hour) was followed by a stabilizing effect and increase of G_C when returned to laboratory conditions (30 % RH at 25 °C).

3.3.3 Stress change in die attach materials

The laminated die-stack has to be mechanically attached to the electronic package with a suitable pressure inlet tube. This can be done by soldering of metallized surfaces or by application of epoxy adhesive. Barometric sensors where the sensor die stack is exposed to the test pressure can also be attached by using a soft Room Temperature Vulcanization (RTV) silicone [62].

The mechanical stress influence from the selected die-attach material should be decoupled from the stress-sensing die by implementing a suitable stress-isolating

structure between the die-attach area and the piezoresistors. An example of this is reported in Article IV.

The use of thermosetting epoxies as die attach material might introduce sensor output-signal drift with temperature change [63-65]. The effect can be especially large during the first thermal cycle after physical aging (or storage) at temperatures below the glass transition temperature (T_g) [66]. This type of aging can be rejuvenated (de-aged) by heating the epoxy above T_g [67].

The mechanical stress in polymers can also be influenced by humidity. The water concentration in the polymer will vary due to diffusion of water in or out of the polymer, depending on the environment. This will result in localized swelling and a time varying mechanical stress depending on the mechanical constraints [68].

3.3.4 Stress change in molded die-stacks

Some sensor designs use molding compounds as a means of protecting the sensor die-stack from the environment, such as silicone [69] or epoxy mold [65, 70, 71]. Due to the high influence on mechanical stress from the packaging materials on the chip-stack, these solutions are generally not suitable for high-stability designs. The stress from the molding compounds will generally be influenced by humidity through hygroscopic swelling [72], as well as physical aging of the polymers.

3.3.5 Stress change due to self-heating

When applying power to a pressure sensor, self-heating will occur in the piezoresistors and it will take some time to accomplish an even temperature distribution across the various materials in the sensor. Local temperature differences will result in a varying mechanical stress, observed at the sensor output-signal. This effect could be significant if the sensor design consists of materials with low thermal conductivity and large differences in the coefficient of thermal expansion (CTE). Silicon has a relatively high thermal conductivity (148 W/m K) as opposed to silicon dioxide (1.4 W/m K) or other ceramics. Polymers normally have a very low thermal conductivity and a high CTE,

resulting in a relative long period of stress change following a temperature change. Polymers are therefore often mixed with other materials to increase the thermal conductivity, when used as adhesives.

Zarnik *et al.* [73] studied warm-up and offset stability of a low-pressure piezoresistive ceramic pressure sensor.

3.4 Pressure change in sealed cavities

3.4.1 Sensor package hermeticity level

A piezoresistive MEMS pressure sensor is typically mounted in a hermetic package in order to protect the internal structure from influence from the environment. The hermeticity levels used by relevant test standards for these packages, such as MIL-STD-883 Test Method (TM) 1014 [74] are motivated by the need to avoid moisture and prevent corrosion during the device lifetime. Leak testing at the package-level is typically done by measuring the rate of helium escape from a sensor package that has been pressurized with helium.

The output signal of a sealed absolute type pressure sensor might also be influenced by the sensor package pressure. The package pressure will result in a mechanical stress in the sensor structure, and any change of the package pressure due to leakage might be observable on the sensor output signal. This might necessitate additional requirements on the sensor package hermeticity levels as discussed in Article II.

3.4.2 Vacuum reference hermeticity level

Several methods of sealing a vacuum reference for a pressure sensor structure has been developed such as glass frit bonding [75], anodic bonding, direct wafer bonding, eutectic bonding, or out-diffusion of hydrogen [76].

Any change of pressure in the vacuum reference cavity of an absolute sensor will be observed as a change in the sensor output signal. The pressure stability of the vacuum reference is therefore extremely important. Due to the normally small volume of vacuum reference cavities and the extremely low leak rates allowed, test methods

used for larger volume methods for leak testing are unsuitable for these cavities [77, 78]. One method that can be used is to observe the stability on the sensor output-signal during a prolonged time using a high over-pressure. Maximum allowed output-signal change during this accelerated test can be calculated from the sensor long-term drift specification using the equations for molecular flow into a sealed cavity [79].

In addition to traditional leak paths through the sealing material or between the sealing material and the silicon/glass dies, gas permeation through either the cavity wall material or the bonding materials [79] might also result in an observable pressure change.

Sparks [80] observed ingress of helium at 23 to 100 °C both for reflowed glass bonded, as well as direct silicon bonded cavities, suggesting diffusion of helium through silicon to be the main cause. Similar effects were not observed for hydrogen, argon or air. Permeation will limit the choice of useable gases for accelerated testing, and also put restrictions on the sensors operating environment.

3.4.3 Outgassing and adsorption

Even with a perfect hermetic seal of the vacuum reference cavity, a small rest-gas pressure might be present after the sealing process. The resulting gas pressure might change over time and temperature due to adsorption and outgassing of gas molecules to/from the materials contained in the cavity.

Residual gas analysis (RGA) done on four samples after a glass-frit sealing process during this work showed a rest-gas pressure of 0.8 to 2.4 hPa in the reference vacuum cavity. The main component was carbon containing gases, probably originating from the organic components of the glass frit material. Knechtel [81] found that a vacuum level of 1-5 hPa can be obtained using glass-frit bonding, while Lorenz *et al.* [82] obtained a rest-gas pressure of 5 hPa using localized laser glass-frit sealing process. Also when using silicon-glass anodic bonding, some oxygen will be released from the glass, resulting in a rest-gas pressure [83]. Schuessler *et al.* [84] has also observed outgassing of hydrogen from plated metal parts.

The effect of a rest-gas pressure on a sensor signal will depend on the outgassing/adsorption time constants. If there is no outgassing/adsorption, the effect is repeatable and included in the overall sensor characteristics during calibration. Outgassing/adsorption with long time-constant will be observed as drift on the output-signal. If the time-constants are of the same order as the thermal cycling period, it will be observed as thermal hysteresis on the output-signal.

One method to reduce the amount of outgassing is to do a proper bake out of the components to be sealed [85]. This consist of keeping the package at an elevated temperature in an ultra-high vacuum for an extended period of time prior to the sealing process.

A method to prevent further outgassing after sealing and maintain a constant low gas pressure is to use a non-evaporable getter (NEG) material for adsorption of the rest-gas [86, 87]. The getter material can be deposited during manufacturing of the cavity structure, and consist of a porous mixture of a Ti and Zr based alloy. The getter material is activated at the bonding temperature and will adsorb most of the remaining active gases in the cavity through oxide and hydride formation as well as simple surface adsorption.

Sparks *et al*. [88] found improved performance for resonators in a glass frit sealed structure when utilizing getter for reduced rest-gas pressure.

4 Contributions of this work

Due to the variety of physical phenomena that can possibly influence the stability of piezoresistive pressure sensors, this study has covered several fields such as semiconductor physics, structural mechanics, fracture mechanics, die/wafer bonding, materials science, environmental influence, low voltage measurements and data analysis. As discussed in section 3, instability of the sensor output-signal can be caused by both electrical, mechanical and leakage related phenomena, and a number of relevant sources should therefore be considered when optimizing a sensor design for high-stability.

4.1 Mechanical stress from die bonding

The sensor structures in this thesis have generally been configured as a die-stack consisting of two or three laminated silicon-dies. The dies were bonded using a glass-frit laminating process, where a non-crystallizing lead silicate glass with a relative low melting point of 330°C was used.

Application of glass frit material can be done either by manual or automatic dispensing or by screen printing. The final resolution and thickness of the deposited glass frit material will be strongly dependent on the deposition process used.

The bonding process will introduce thermal stress, affecting the mechanical stress distribution in the sensor. The studied glass frit material contains a large proportion of lead oxide, and we found that the use of X-ray Computed Tomography (CT) was highly efficient for characterization of glass frit distribution in fabricated samples. An example of observed glass-frit distribution is shown in Figure 16 where the silicon material has been removed in software and the shape of the upper and lower glass frit bonds are identified. A reconstructed cross section is shown in Figure 17 identifying two anomalies termed *excess material* and *recessed edge* which were studied in detail.

Based on these and similar observations from a number of samples, a simulation study was initiated to study potential effects of packaging-induced stress on the sensor performance. Typically observed variations of 50 µm was used for *excess material*, and 145 µm was used for the *recessed edge* variation. It was demonstrated that a model based on observed variations of glass frit material distribution in fabricated samples give rise to offset variations that were consistent with observed offset values. Initial results were published in Article I.

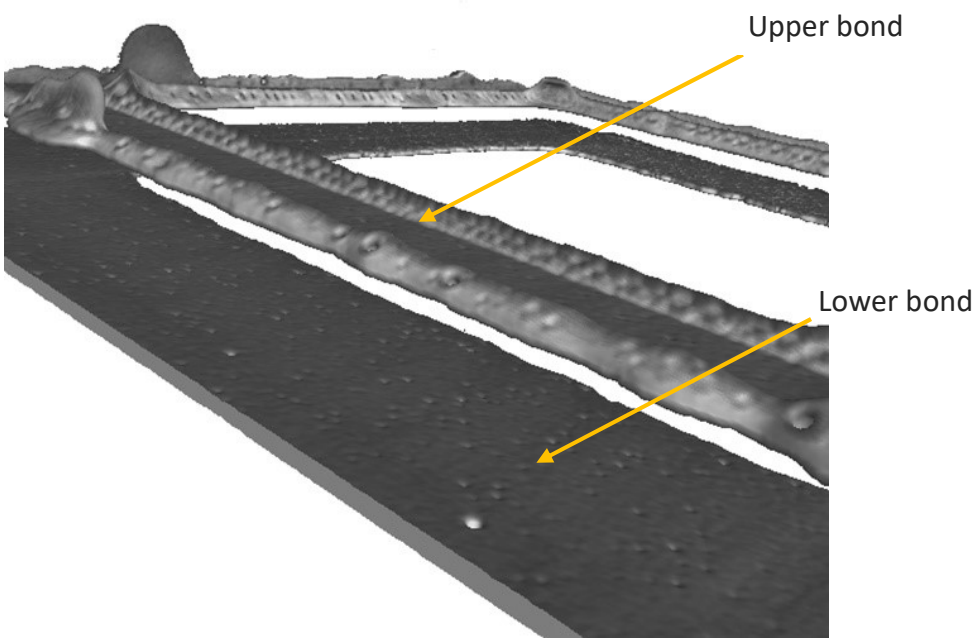

Figure 16 X-ray CT example showing glass frit material only in a laminated die-stack.

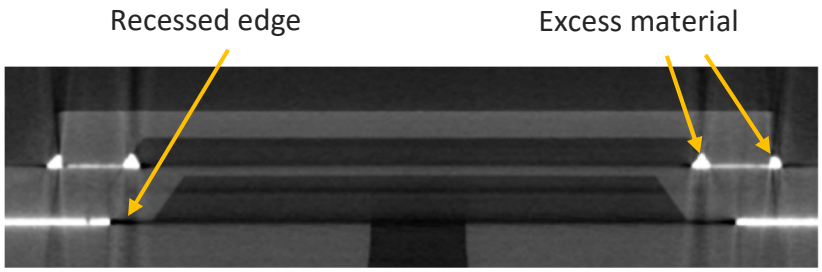

Figure 17 X-ray Computed Tomography (CT) cross section of glass frit laminated die-stack showing recessed edge and excess material anomalies (from Article I)
White region: glass frit. Gray region: silicon. Black region: air/vacuum.

Following the initial modelling for Article I, the study was extended to also include analysis of TCO changes in addition to the zero-point. A major part of TCO was shown to be caused by thermo-mechanical stress in the excess glass frit. Using a new technology for optimized glass frit screen-printing, we were able to verify the modelling by measurements. Significant reductions in mechanical stress from the glass frit material was obtained, resulting in a reduction of the influence on both the sensor zero-point as well as on the TCO. The reduced TCO results in lower temperature sensitivity and also a reduced thermal hysteresis.

At the core of this work, detailed finite element models for analysis of the mechanical stress distribution were built using COMSOL Multiphysics simulation software. Figure 18 shows an example of the modelled x-axis normal stress (σ_x) distribution through a cross section for an absolute sensor model with minimum excess glass frit material. Figure 19 is a similar plot, but for a sensor with maximum excess glass frit and an recessed edge. By probing both σ_x and σ_y at the piezoresistor positions, we used the differential stress ($\sigma_x - \sigma_y$) for calculation of the resulting zero-point change.

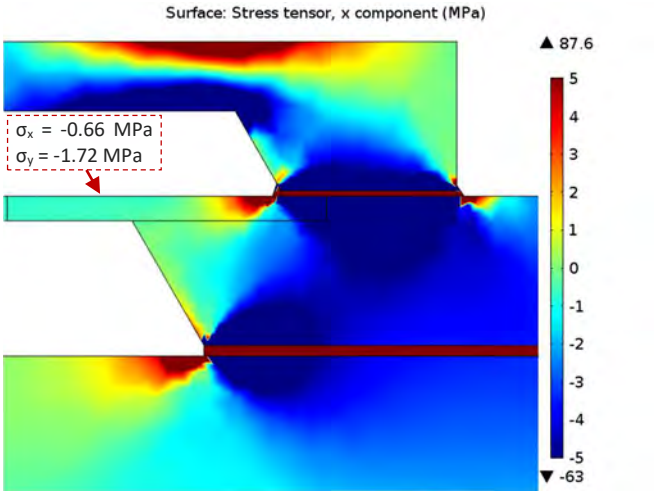

Figure 18 x-axis normal stress (σ_x) distribution for model with minimum excess material (color range: ± 5 MPa) (From Article III)

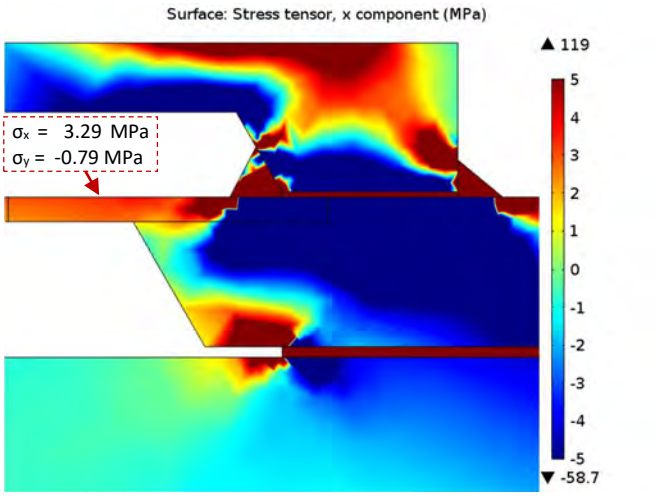

Figure 19 x-axis normal stress (σ_x) distribution for model with maximum excess material and recessed edge (color range: ± 5 MPa) (From Article III)

The results of optimizing the glass frit material distribution is illustrated in Figure 20 showing measurement results for both zero-point and TCO for three sensor variants. The original absolute sensor design with excess glass frit (labeled *ABS*) experienced a large negative zero-point and high TCO due to mechanical stress from the bonding material. This effect was significantly reduced for the absolute sensor with the optimized glass frit distribution (labeled *ABS opt.*). For reference, Figure 20 also show

results for a two-die differential sensor (labeled *DIFF*) where no reference die is present and both zero-point and TCO have a distribution around zero.

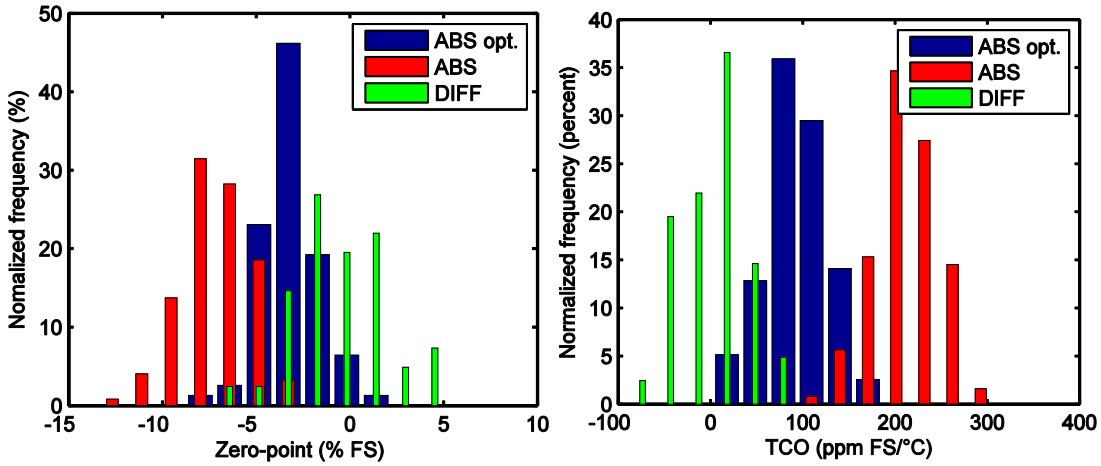

Figure 20 Zero-point and TCO from manufacturing measurements of three sensor versions: absolute sensor with large excess glass frit (ABS, 124 samples), absolute sensor with optimized glass frit (ABS opt, 84 samples) and a differential sensor (DIFF, 41 samples) (From Article III)

Glass-frit regions with high tensile stress-levels could be subjectable to stress relaxation in the form of microcrack formation. We therefore performed a series of thermal cycling experiments, optical micrograph observations as well as additional modelling focusing on the development of microcracks in the glass frit material as a root cause for observed anomalies. The results were published in Article III.

This optimized glass frit printing process has been implemented in manufacturing of new sensors during the project. Production measurements from several thousand sensors confirm the modelled change in stress distribution. We also observe an increased stability, attributed to a reduced occurrence of microcracks.

The glass frit bonding process is currently done on die level. Significant cost reduction is possible if we are able to do the bonding on wafer level. We have therefore also studied alternative bonding processes in the 4P-project, such as thin-film anodic bonding. Results from this is not part of this thesis, but mechanical stability of the

die/wafer bond will continue to be a central subject in defining the reliability and stability of a bonded sensor assembly.

4.2 Leak related mechanical stress

Monocrystalline silicon is regarded as a perfectly elastic material and is therefore used as a diaphragm in MEMS pressure sensors. A differential pressure across the diaphragm results in slight bending with resulting mechanical stress at the piezoresistor regions. Any changes of the gas pressure surrounding die-stack might also influence the mechanical stress at the piezoresistor positions. Figure 21 shows a principle cross section of an absolute pressure sensor consisting of a triple stack of glass frit bonded silicon dies mounted in a sealed TO-8 can. The cap pressure *P_cap* is constant for a constant temperature, but any temperature change will also change *P_cap*, following the ideal gas law. With zero leakage between *P_cap* and the surrounding ambient pressure *P_ambient* or the test pressure *P_test*, any changes in *P_cap* due to temperature changes are repeatable, and any influence on the measured signal will then also be repeatable. It can then easily be accommodated for during sensor calibration.

If there is a leak path from the cap cavity to either the ambient or the test pressure cavity, *P_cap* will change over time, possibly influencing the sensor output-signal.

Established industrial hermeticity requirements for electronic devices with internal cavities, such as MIL-STD-883 Test Method 1014, are typically motivated by the need to avoid moisture in sealed devices. However, the output signal of a sealed pressure-sensor structure will also be influenced by the sensor cap pressure, putting additional requirements on the sensor package hermeticity in order to guarantee a stable operation under variable conditions.

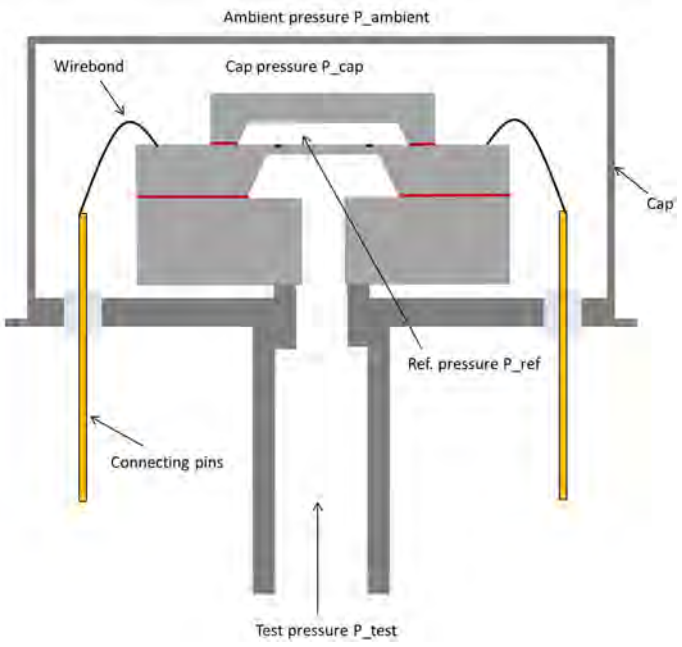

Figure 21 Principle cross section through an absolute pressure sensor mounted in a TO-8 can (from Article II)

A detailed modelling of the sensor structure and associated pressures in Figure 21 was performed, with a resulting sensitivity of the output signal to a varying cap pressure of S_{cap} = -0.25 %FS/bar. This was also confirmed by experimental verification. When this behavior is known, it will put additional requirement on the package hermeticity level to keep the sensor design within the drift specification under varying environmental conditions.

It was found that hermeticity levels typically used to avoid moisture in electronic packages can be insufficient when targeting control of long-term drift related mechanisms. We also showed that the presence of a condensing gas, such as water vapor will change the temperature characteristics of the sensor output-signal. The added water vapor will increase the dew point in the sensor cap. At temperatures above the dew point, all water present is in gaseous form, and the partial pressure can be calculated by the ideal gas law. At temperatures below the dew point, parts of the water will condense and the partial pressure of the remaining water vapor will be strongly temperature dependent following the curve for saturated vapor pressure versus temperature as stated in [89].

The results can be used for failure analysis for detection of small cap leak related phenomena and were published in Article II.

4.3 Mechanical stress from die attach materials

It is common practice to characterize pressure sensors and other electronic components versus temperature by using a thermal chamber. Even when studying packaging related stress [70, 71], the humidity levels during thermal cycling is seldom mentioned.

By observing the relative humidity levels in thermal chambers during thermal cycling, we have found that the humidity will experience significant variation during one thermal cycle, and there are large variations between different chamber models. Figure 22 shows measured relative humidity versus temperature during three identical thermal cycles for two different thermal chambers.

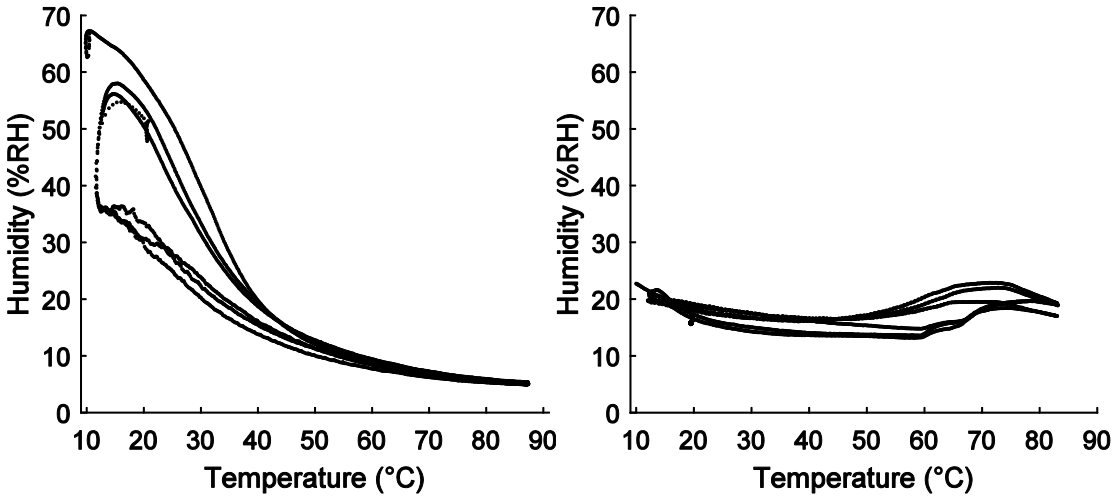

Figure 22 Relative humidity versus temperature during three identical thermal cycles for two different thermal chambers

While the leftmost plot shows a decreasing relative humidity level versus temperature, the rightmost plot shows a fairly constant relative humidity level versus temperature. Note that a constant relative humidity over temperature means that the absolute partial pressure of the water vapor is increasing with temperature, while a decreasing

relative humidity means that the absolute partial water pressure has less variation with temperature.

The exact humidity levels will be dependent on the environmental conditions, type of thermal chamber, dry gas flow, temperature ramping speed etc. If a design is sensitive to humidity, the effect of this inherent humidity-cycling will affect the measurements and might be misinterpreted as thermal hysteresis.

Some pressure sensors will show an increase of the zero-point when stored for weeks at ambient conditions. When thermally cycled, they show a first-cycle effect, where the deviation from calibrated signal output is reduced to normal levels during the first heating to elevated temperatures.

In addition, we have observed that some sensors experienced an unexpected temperature and time dependent signal-change when subjected to a change of relative humidity, as illustrated in Figure 23 for one specific sensor variant at 30, 40 and 50 °C after a humidity step from 15 %RH to 60 %RH.

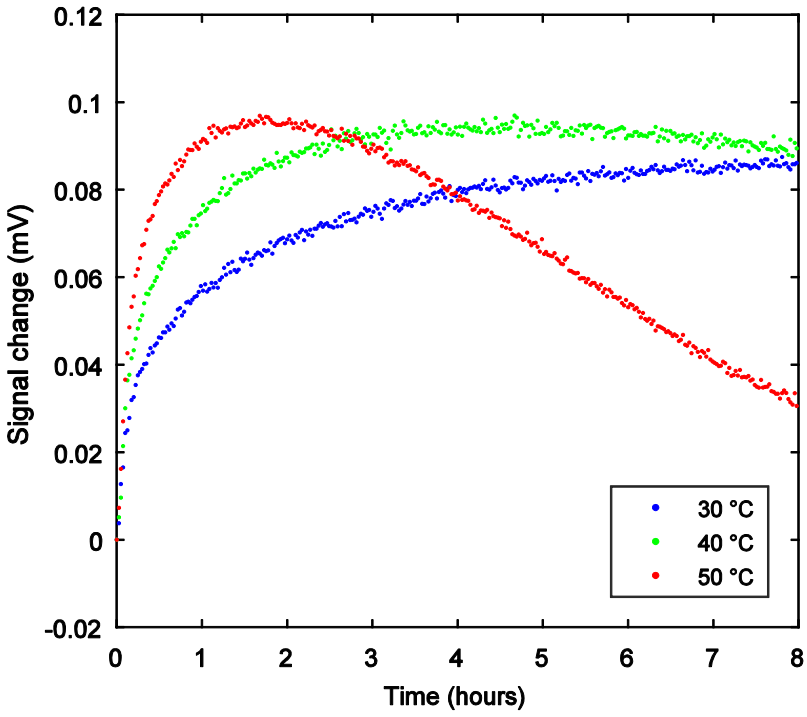

Figure 23 Example of measured signal change for a P203 sensor after humidity step from 15 %RH to 60 %RH for 30, 40 and 50 °C (From Article IV)

This behavior was studied in the work published as Article IV in this thesis, where we found that physical aging combined with diffusion of water in the epoxy die attach material could explain the observed behavior. Since the epoxy die attach material in the sensor is constrained by the sensor structure, diffusion of water will result in localized swelling that is coupled to mechanical stress at the piezoresistor positions. Influence from moisture will be stabilized when a new water concentration has been established throughout the epoxy material, but the exact behavior is complicated by physical aging as well as moisture dependent material parameters.

Instead of the term 'thermal hysteresis', we therefore introduced the term 'hygro-thermal hysteresis' for describing the observed behavior. By the use of finite element analysis, we modelled water diffusion in the epoxy material coupled with localized swelling. The calculated stress was converted to zero-point influence for three sensor geometries containing different support die designs. One of these was the stress-isolating support die as shown in Figure 24, designed and fabricated during the project period. Experiments and modelling verified that with the new stress-isolating support die, mechanical stress from the epoxy material could be reduced to neglectable levels.

Fabrication of this support die proved to be challenging as it required a 700 µm deep reactive ion etching (DRIE) from both sides of the support wafer, but we got enough samples to demonstrate the stress-isolating performance.

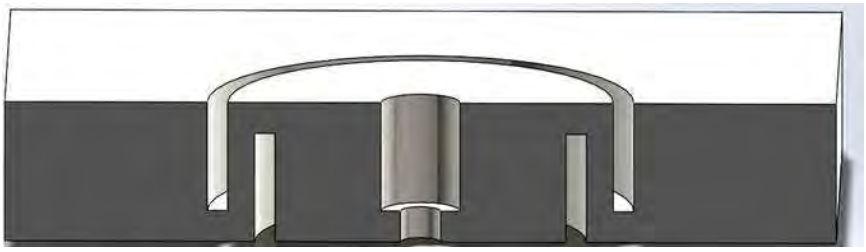

Figure 24 Cross section view of stress-isolating support die model

4.4 Mechanical stress from metallization

Thermo-mechanical stress from thin-film metallization can cause thermal hysteresis in a sensor output signal [41]. The large difference in CTE of silicon and aluminum thin

film metallization will result in significant thermo-mechanical stress, and there is a possibility that this can also affect the stress at the piezoresistor positions.

In this project, an existing sensor wafer-design was modified. All production steps of the original sensor wafers were kept, except for the last two mask layers: *contact hole definition* and *metallization*. With these limitations, a number of test-sensor variants and structures were designed, including variants for metal layout optimizations as well as for studying possible influence from surface charge on sensor behavior.

One of the test-structures, named M3, contained 4 strips of metal, located on the oxide directly above two of the piezoresistors for maximizing the influence from metallization. By maximizing the influence from metallization, it is possible to compare mechanical properties of different metal alloys and deposition parameters, as well as the effect of annealing conditions. Details from this experiment are included as Article V.

4.5 Measurement setup

In the measurement setup used for parts of this work, up to 20 pressure-sensors were mounted on test-cards and placed in a computer controlled environmental test-chamber. They were connected through cable assemblies to an interfacing electronics module located outside the test-chamber. This module provided excitation current to the sensors and interfacing to a combined multiplexer/DMM module. Temperature and humidity sensors were added for accurate measurement of environmental conditions, and a computer controlled pressure controller was used for pressure control.

A flexible software platform was used for accurate control of temperature, humidity and pressure, and all measurements were stored in a SQL database for further analysis.

100 ppm of full scale (FS) with a FS of 115 mV is 11.5 µV. Accurate measurement of signal changes of the order of µV during thermal and humidity cycling can be challenging, with several possible error sources also from the measurement setup.

Measurement cable assemblies can be sensitive to both temperature and humidity, resulting in large variations of impedance. Especially when providing excitation voltages thru the same cable, or when the measured signal contains a common mode component (as in a Wheatstone bridge), small leakage currents between the individual conductors in the cable might cause anomalies. It is therefore important to use quality cables with known performance for the test-environment used.

Thermoelectric voltages or thermoelectric EMF (Electro-Motive Force) are a common source of errors for low-voltage measurements [90]. It results from a temperature difference at junctions between two dissimilar materials with a magnitude determined by the relative Seebeck coefficient (Q_{AB}). The temperature difference can for example be caused by thermal flow from the hot environment in the thermal chamber through the cable assembly connecting the sensors to the measurement equipment located at room temperature. While a crimped Cu-Cu connection may have $Q_{AB} \leq 0.2$ µV/°C, the Seebeck coefficient is increased to 1-3 µV/°C for Cu-Pb/Sn (soldered connection) and it can be as high as 1000 µV/°C for Cu-CuO (oxidiced connection) [91]. Keeping the connectors free of contamination and oxidation is therefore extremely important.

By replacing the sensors with fixed resistors and characterizing the zero-signal of the measurement setup over temperature, first without and then with an excitation voltage present, possible thermoelectric EMF contribution as well as contributions from leak currents can be quantified.

5 Concluding remarks

In this work, we have studied small variations in sensor performance that are normally treated as normal process variations and uncertainty. We have been able to isolate and explain these variations through experimental work and modelling, and demonstrated corrective changes to reduce these effects.

We have modelled and experimentally verified the relation between glass frit material distribution, the sensor zero-point and the TCO. Stress relaxation in the form of microcrack-induced signal changes has also been studied in detail. An optimized material distribution has been modelled and experimentally verified.

Hygro-thermo-mechanical stress from a thermoset die-attach material has been identified as a source for both a first-cycle effect after storage as well as hygro-thermal hysteresis. A stress-isolating support die has been designed and manufactured, reducing the influence from the die-attach material to neglectable levels.

In addition, studies have been performed on both leak related mechanical stress effects as well as stress from metallization.

Based on this research, MEMSCAP is now able to manufacture pressure sensors with an improved accuracy and stability, and observed anomalies can be understood and explained. Some of the suggested improvements from this work have already been implemented in the sensor manufacturing, while others are planned for future design changes.

Focusing on physical properties possibly influencing the stability of piezoresistive sensors through the project period, has resulted in valuable insight into the various contributing factors.

Although the published articles are specific to pressure sensors, we expect that the content will be of interest also for researchers working with other types of sensors.

References

[1] J. C. Doll, and B. L. Pruitt, *Piezoresistor Design and Applications*: Springer New York, 2013.

[2] "NASA JPL Mars Science Laboratory - Tunable Laser Spectrometer," 1, 2017; http://microdevices.jpl.nasa.gov/news/news-tunable-laser-spectrometer.php.

[3] "Carmat artificial heart prosthesis," 1, 2017; http://www.carmatsa.com/en/carmat-heart/technology/prosthesis.

[4] "Reduced Vertical Separation Minimum (RVSM)," 3, 2017; https://www.faa.gov/air_traffic/separation_standards/rvsm/.

[5] C. S. Smith, "Piezoresistance Effect in Germanium and Silicon," *Physical Review,* vol. 94, no. 1, pp. 42-49, 04/01/, 1954.

[6] D. Neamen, *Semiconductor Physics And Devices*: Mc Graw-Hill, 2012.

[7] R. S. Muller, T. I. Kamins, M. Chan, and P. K. Ko, *Device electronics for integrated circuits*, 1986.

[8] M. M. Atalla, A. R. Bray, and R. Lindner, "Stability of thermally oxidized silicon junctions in wet atmospheres," *Proceedings of the IEE - Part B: Electronic and Communication Engineering,* vol. 106, no. 17, pp. 1130-1137, 1959.

[9] W. Shockley, W. W. Hooper, H. J. Queisser, and W. Schroen, "Mobile electric charges on insulating oxides with application to oxide covered silicon p-n junctions," *Surface Science,* vol. 2, pp. 277-287, 1964/01/01, 1964.

[10] E. Kooi, *The surface properties of oxidized silicon*: Springer, 1967.

[11] P. Ho, K. Lehovec, and L. Fedotowsky, "Charge motion on silicon oxide surfaces," *Surface Science,* vol. 6, no. 4, pp. 440-460, 1967/04/01, 1967.

[12] E. S. Schlegel, G. L. Schnable, R. F. Schwarz, and J. P. Spratt, "Behavior of surface ions on semiconductor devices," *Electron Devices, IEEE Transactions on,* vol. 15, no. 12, pp. 973-979, 1968.

[13] B. Martin, A. Rathi, and H. Kliem, "Surface charging of silicondioxide/silicon structures," *Dielectrics and Electrical Insulation, IEEE Transactions on,* vol. 19, no. 4, pp. 1124-1131, 2012.

[14] W.-T. Park, B. Grote, C. Dawson, and L. Liu, "Surface charge extraction methods in offset shift-related failures of MEMS pressure sensors," *Journal of Micromechanics and Microengineering,* vol. 20, no. 11, pp. 115027, 2010.

[15] J. A. Voorthuyzen, K. Keskin, and P. Bergveld, "Investigations of the surface conductivity of silicon dioxide and methods to reduce it," *Surface Science,* vol. 187, no. 1, pp. 201-211, 8/2/, 1987.

[16] K. Sager, G. Gerlach, A. Nakladal, and A. Schroth, "Ambient humidity and moisture — a decisive failure source in piezoresistive sensors," *Sensors and Actuators A: Physical,* vol. 46, no. 1–3, pp. 171-175, 1//, 1995.

[17] A. Nakladal, K. Sager, and G. Gerlach, "Influences of humidity and moisture on the long-term stability of piezoresistive pressure sensors," *Measurement,* vol. 16, no. 1, pp. 21-29, 9//, 1995.

[18] H. Bentarzi, A. Zitouni, and Y. Kribes, "Oxide charges densities determination using charge-pumping technique with BTS in MOS structures," *WSEAS Transactions on electronics,* vol. 5, no. No 4 (2008), pp. 101-110, 2008.
[19] K. E. Holbert, J. A. Nessel, S. S. McCready, A. S. Heger, and T. H. Harlow, "Response of piezoresistive MEMS accelerometers and pressure transducers to high gamma dose," *IEEE Transactions on Nuclear Science,* vol. 50, no. 6, pp. 1852-1859, 2003.
[20] Y. Wakashima, H. Inayoshi, K. Nishi, and S. Nishida, "A Study of Parasitic MOS Formation Mechanism in Plastic Encapsulated MOS Devices," *Reliability Physics Symposium, 1976. 14th Annual*, pp. 223-227, April 1976, 1976.
[21] H. Jakobsen, and O. Solgaard, "Bulk piezoresistors for stable pressure sensors," *12th Nordic Semiconductor Meeting*, pp. 271-274, 8-11 June 1986, 1986.
[22] J. F. Marshall, *Stress sensor apparatus*,to Honeywell Inc., 1978.
[23] M. Esashi, H. Komatsu, and T. Matsuo, "Biomedical pressure sensor using buried piezoresistors," *Sensors and Actuators,* vol. 4, pp. 537-544, 1983/01/01, 1983.
[24] C. Gang, L. Chaojun, L. Xiaogang, W. Xuefang, and L. Sheng, "Resistance electric filed dependence simulation of piezoresistive silicon pressure sensor and improvement by shield layer," *Thermal, Mechanical and Multi-Physics Simulation and Experiments in Microelectronics and Microsystems (EuroSimE), 2013 14th International Conference on*, pp. 1-4, 14-17 April 2013, 2013.
[25] Y. Murakami, and T. Shingyouji, "Separation and analysis of diffusion and generation components of pn junction leakage current in various silicon wafers," *Journal of Applied Physics,* vol. 75, no. 7, pp. 3548-3552, 1994.
[26] Y. C. Sun, Z. Gao, L. Q. Tian, and Y. Zhang, "Modelling of the reverse current and its effects on the thermal drift of the offset voltage for piezoresistive pressure sensors," *Sensors and Actuators A: Physical,* vol. 116, no. 1, pp. 125-132, 10/4/, 2004.
[27] M. Nakajima, K. Kuwabara, T. Ishihara, T. Sakata, M. Usui, N. Nemoto, E. Hashimoto, J. Yamaguchi, S. Uchiyama, and Y. Jin, "A physical modeling and long-term measurement of tilting angle drift caused by dielectric surface charging in MEMS micromirrors," *Optical MEMS and Nanophotonics (OMN), 2013 International Conference on*, pp. 19-20, 18-22 Aug. 2013, 2013.
[28] S. Bouwstra, F. R. Blom, T. S. J. Lammerink, H. Yntema, P. Schrap, J. H. J. Fluitman, and M. Elwenspoek, "Excitation and detection of vibrations of micromechanical structures using a dielectric thin film," *Sensors and Actuators,* vol. 17, no. 1, pp. 219-223, 1989/05/03, 1989.
[29] J. H. T. Ransley, C. Durkan, and A. A. Seshia, "A Depletion Layer Actuator," *Solid-State Sensors, Actuators and Microsystems Conference, 2007. TRANSDUCERS 2007. International*, pp. 1393-1396, 10-14 June 2007, 2007.
[30] A. Andrei, C. Malhaire, S. Brida, and D. Barbier, "Long-Term Stability of Metal Lines, Polysilicon Gauges, and Ohmic Contacts for Harsh-Environment Pressure Sensors," *Sensors Journal, IEEE,* vol. 6, no. 6, pp. 1596-1601, 2006.
[31] J. R. Lloyd, and R. H. Koch, "Study of electromigration-induced resistance and resistance decay in Al thin-film conductors," *Applied Physics Letters,* vol. 52, no. 3, pp. 194-196, 1988.
[32] B. Marz, S. Scheibe, A. Graff, and M. Petzold, "Growth behaviour of gold-aluminum intermetallic phases (IMP) in temperature aged ball bonds observed

by electron backscatter diffraction," *Electronic System-Integration Technology Conference (ESTC), 2010 3rd*, pp. 1-4, 13-16 Sept. 2010, 2010.

[33] E. Philofsky, and E. Hall, "A Review of the Limitations of Aluminum Thin Films on Semiconductor Devices," *Parts, Hybrids, and Packaging, IEEE Transactions on,* vol. 11, no. 4, pp. 281-290, 1975.

[34] E. Zin, N. Michael, S. H. Kang, K. H. Oh, U. Chul, J. S. Cho, J. T. Moon, and C. U. Kim, "Mechanism of electromigration in Au/Al wirebond and its effects," *Electronic Components and Technology Conference, 2009. ECTC 2009. 59th*, pp. 943-947, 26-29 May 2009, 2009.

[35] M. Hershkovitz, I. A. Blech, and Y. Komem, "Stress relaxation in thin aluminium films," *Thin Solid Films,* vol. 130, no. 1–2, pp. 87-93, 8/16/, 1985.

[36] D. S. Gardner, and P. A. Flinn, "Mechanical stress as a function of temperature in aluminum films," *Electron Devices, IEEE Transactions on,* vol. 35, no. 12, pp. 2160-2169, 1988.

[37] Y. L. Shen, and S. Suresh, "Thermal cycling and stress relaxation response of Si-Al and Si-Al-SiO2 layered thin films," *Acta Metallurgica et Materialia,* vol. 43, no. 11, pp. 3915-3926, 11//, 1995.

[38] P. A. Flinn, D. S. Gardner, and W. D. Nix, "Measurement and Interpretation of Stress in Aluminum-Based Metallization as a Function of Thermal History," *IEEE Transactions on Electron Devices,* vol. ED-34, no. 3, pp. 689-699, 1987.

[39] M. A. Korhonen, C. A. Paszkiet, and C. Y. Li, "Mechanisms of thermal stress relaxation and stress-induced voiding in narrow aluminum-based metallizations," *Journal of Applied Physics,* vol. 69, no. 12, pp. 8083-8091, 1991.

[40] W. M. Kuschke, and E. Arzt, "Investigation of the stresses in continuous thin films and patterned lines by x-ray diffraction," *Applied Physics Letters,* vol. 64, no. 9, pp. 1097-1099, 1994.

[41] J. A. Chiou, and S. Chen, "Thermal Hysteresis Analysis of MEMS Pressure Sensors," *Microelectromechanical Systems, Journal of,* vol. 14, no. 4, pp. 782-787, 2005.

[42] C. Malhaire, and D. Barbier, "Design of a polysilicon-on-insulator pressure sensor with original polysilicon layout for harsh environment," *Thin Solid Films,* vol. 427, no. 1–2, pp. 362-366, 3/3/, 2003.

[43] I. Blech, and U. Cohen, "Effects of humidity on stress in thin silicon dioxide films," *Journal of Applied Physics,* vol. 53, no. 6, pp. 4202-4207, 1982.

[44] M. T. A. Saif, S. Zhang, A. Haque, and K. J. Hsia, "Effect of native Al2O3 on the elastic response of nanoscale Al films," *Acta Materialia,* vol. 50, no. 11, pp. 2779-2786, 6/28/, 2002.

[45] C. Dresbach, A. Krombholz, M. Ebert, and J. Bagdahn, "Mechanical properties of glass frit bonded micro packages," *Microsystem Technologies,* vol. 12, no. 5, pp. 473-480, 2006/04/01, 2006.

[46] M. Petzold, C. Dresbach, M. Ebert, J. Bagdahn, M. Wiemer, K. Glien, J. Graf, R. Muller-Fiedler, and H. Hofer, "Fracture mechanical life-time investigation of glass frit-bonded sensors," *Thermal and Thermomechanical Phenomena in Electronics Systems, 2006. ITHERM '06. The Tenth Intersociety Conference on*, pp. 1343-1348, May 30 2006-June 2 2006, 2006.

[47] F. Naumann, S. Brand, M. Bernasch, S. Tismer, P. Czurratis, D. Wunsch, and M. Petzold, "Advanced characterization of glass frit bonded micro-chevron-test

samples based on scanning acoustic microscopy," *Microsystem Technologies-Micro-and Nanosystems-Information Storage and Processing Systems,* vol. 19, no. 5, pp. 689-695, May, 2013.

[48] K. Notzold, J. Graf, and R. Muller-Fiedler, "A four-point-bending-test for the stability assessment of glass frit bonded molded microsensors," *Microelectronics Reliability,* vol. 48, no. 8-9, pp. 1562-1566, Aug-Sep, 2008.

[49] K. Glien, "Dichtheit und Lebensdauer Glas-Frit gebondeter mikromechanischer Inertialsensoren," Fakultät für Maschinenbau (MACH), Institut für Zuverlässigkeit von Bauteilen und Systemen (IZBS), Karlsruhe, 2007.

[50] B. Boettge, C. Dresbach, A. Graff, M. Petzold, and J. Bagdahn, "Mechanical Characterization and Micro Structure Diagnostics of Glass Frit Bonded Interfaces," *ECT Transactions*, 2008.

[51] Q. Cai, A. Bhunia, C. Tsai, M. W. Kendig, and J. F. DeNatale, "Studies of material and process compatibility in developing compact silicon vapor chambers," *Journal of Micromechanics and Microengineering,* vol. 23, no. 6, pp. 065003, 2013.

[52] R. Knechtel, "Chapter Thirty Three - Glass Frit Bonding," *Handbook of Silicon Based MEMS Materials and Technologies*, V. Lindroos, M. Tilli, A. Lehto and T. Motooka, eds., pp. 521-531, Boston: William Andrew Publishing, 2010.

[53] P. Ramm, J. J.-Q. Lu, and M. M. V. Taklo, *Handbook of wafer bonding*, Weinheim: Wiley-VCH, 2012.

[54] S. W. Freiman, S. M. Wiederhorn, and J. J. Mecholsky Jr, "Environmentally enhanced fracture of glass: A historical perspective," *Journal of the American Ceramic Society,* vol. 92, no. 7, pp. 1371-1382, 2009.

[55] M. Ciccotti, "Stress-corrosion mechanisms in silicate glasses," *Journal of Physics D: Applied Physics,* vol. 42, no. 21, pp. 214006, 2009.

[56] S. M. Wiederhorn, and L. H. Bolz, "Stress Corrosion and Static Fatigue of Glass," *Journal of the American Ceramic Society,* vol. 53, no. 10, pp. 543-548, 1970.

[57] A. R. Akisanya, and N. A. Fleck, "Brittle fracture of adhesive joints," *International Journal of Fracture,* vol. 58, no. 2, pp. 93-114, 1992/11/01, 1992.

[58] J. Bagdahn, and M. Petzold, "Fatigue of directly wafer-bonded silicon under static and cyclic loading," *Microsystem Technologies,* vol. 7, no. 4, pp. 175-182, 2001/11/01, 2001.

[59] V. Masteika, J. Kowal, N. S. J. Braitwaite, and T. Rogers, "The effect of atmospheric moisture on crack propagation in the interface between directly bonded silicon wafers," *Microsystem Technologies,* vol. 19, no. 5, pp. 705-712, 2013/05/01, 2013.

[60] F. Fournel, C. Martin-Cocher, D. Radisson, V. Larrey, E. Beche, C. Morales, P. A. Delean, F. Rieutord, and H. Moriceau, "Water Stress Corrosion in Bonded Structures," *ECS Journal of Solid State Science and Technology,* vol. 4, no. 5, pp. P124-P130, January 1, 2015, 2015.

[61] K. Kern, "Stabilität von Glaslotbondverbindungen für mikromechanische Sensoren," Fakultät für Maschinenbau, Karlsruher Institut für Technologie (KIT), Karlsruhe, 2011.

[62] J. K. Reynolds, D. Catling, R. C. Blue, N. I. Maluf, and T. Kenny, "Packaging a piezoresistive pressure sensor to measure low absolute pressures over a wide

sub-zero temperature range," *Sensors and Actuators A: Physical,* vol. 83, no. 1, pp. 142-149, 2000.

[63] R. de Reus, C. Christensen, S. Weichel, S. Bouwstra, J. Janting, G. Friis Eriksen, K. Dyrbye, T. Romedahl Brown, J. P. Krog, O. Søndergård Jensen, and P. Gravesen, "Reliability of industrial packaging for microsystems," *Microelectronics Reliability,* vol. 38, no. 6–8, pp. 1251-1260, 6//, 1998.

[64] M. S. Zarnik, D. Rocak, and S. Macek, "Residual stresses in a pressure-sensor package induced by adhesive material during curing: a case study," *Sensors and Actuators A: Physical,* vol. 116, no. 3, pp. 442-449, 10/29/, 2004.

[65] R. H. Krondorfer, and Y. K. Kim, "Packaging Effect on MEMS Pressure Sensor Performance," *IEEE Transactions on Components and Packaging Technologies,* vol. 30, no. 2, pp. 285-293, 2007.

[66] J. Thurn, and T. Hermel-Davidock, "Thermal stress hysteresis and stress relaxation in an epoxy film," *Journal of Materials Science,* vol. 42, no. 14, pp. 5686-5691, Jul, 2007.

[67] G. M. Odegard, and A. Bandyopadhyay, "Physical aging of epoxy polymers and their composites," *Journal of Polymer Science Part B: Polymer Physics,* vol. 49, no. 24, pp. 1695-1716, 2011.

[68] R. Liu, H. Wang, J. Wang, H. Lee, S. B. Park, X. Xue, Y. Kim, S. Saiyed, and D. Sengupta, "Moisture Diffusion and Hygroscopic Swelling of Adhesives in Electronics Packaging," *2016 IEEE 66th Electronic Components and Technology Conference (ECTC)*, pp. 2203-2209, May 31 2016-June 3 2016, 2016.

[69] T.-L. Chou, C.-H. Chu, C.-T. Lin, and K.-N. Chiang, "Sensitivity analysis of packaging effect of silicon-based piezoresistive pressure sensor," *Sensors and Actuators A: Physical,* vol. 152, no. 1, pp. 29-38, 5/21/, 2009.

[70] J. B. N. ther, A. Larsen, B. Liverød, and P. Ohlckers, "Measurement of package-induced stress and thermal zero shift in transfer molded silicon piezoresistive pressure sensors," *Journal of Micromechanics and Microengineering,* vol. 8, no. 2, pp. 168, 1998.

[71] X. Zhang, S. Park, and M. W. Judy, "Accurate Assessment of Packaging Stress Effects on MEMS Sensors by Measurement and Sensor-Package Interaction Simulations," *Journal of Microelectromechanical Systems,* vol. 16, no. 3, pp. 639-649, 2007.

[72] E. H. Wong, R. Rajoo, S. W. Koh, and T. B. Lim, "The Mechanics and Impact of Hygroscopic Swelling of Polymeric Materials in Electronic Packaging," *Journal of Electronic Packaging,* vol. 124, no. 2, pp. 122-126, 2002.

[73] M. S. Zarnik, D. Belavic, and S. Macek, "The warm-up and offset stability of a low-pressure piezoresistive ceramic pressure sensor," *Sensors and Actuators a-Physical,* vol. 158, no. 2, pp. 198-206, Mar, 2010.

[74] "MIL-STD 883, Method 1014," United States of America, Department of Defence, 2014.

[75] W. Guoqiang, X. Dehui, S. Xiao, X. Bin, and W. Yuelin, "Wafer-Level Vacuum Packaging for Microsystems Using Glass Frit Bonding," *Components, Packaging and Manufacturing Technology, IEEE Transactions on,* vol. 3, no. 10, pp. 1640-1646, 2013.

[76] M. Esashi, S. Sugiyama, K. Ikeda, Y. Wang, and H. Miyashita, "Vacuum-sealed silicon micromachined pressure sensors," *Proceedings of the IEEE,* vol. 86, no. 8, pp. 1627-1639, 1998.
[77] R. C. Kullberg, A. Jonath, and R. K. Lowry, "The unsettled world of leak rate physics: 1 atm large-volume considerations do not apply to MEMS packages: a practitioner's perspective," *SPIE MOEMS-MEMS,* vol. 8250, pp. 82500H-82500H-7, 2012.
[78] S. Costello, M. P. Y. Desmulliez, and S. McCracken, "Review of test methods used for the measurement of hermeticity in packages containing small cavities," *IEEE Transactions on Components, Packaging and Manufacturing Technology,* vol. 2, no. 3, pp. 430-438, 2012.
[79] H. Greenhouse, *Hermeticity of Electronic Packages*: Noyes Publications / William Andrew Publishing, LLC, 1999.
[80] D. Sparks, "The hermeticity of sealed microstructures under low temperature helium and hydrogen exposure," *Journal of Micromechanics and Microengineering,* vol. 23, no. 1, pp. 015016, 2013.
[81] R. Knechtel, "Glass frit bonding: an universal technology for wafer level encapsulation and packaging," *Microsystem Technologies,* vol. 12, no. 1-2, pp. 63-68, 2005/12/01, 2005.
[82] N. Lorenz, S. Millar, M. Desmulliez, and D. P. Hand, "Hermetic glass frit packaging in air and vacuum with localized laser joining," *Journal of Micromechanics and Microengineering,* vol. 21, no. 4, pp. 045039, 2011.
[83] T. Rogers, and J. Kowal, "Selection of glass, anodic bonding conditions and material compatibility for silicon-glass capacitive sensors," *Sensors and Actuators A: Physical,* vol. 46, no. 1–3, pp. 113-120, 1//, 1995.
[84] P. Schuessler, and D. Feliciano-Welpe, *The Effects of Hydrogen On Device Reliability*.
[85] A. R. Schofield, A. A. Trusov, and A. M. Shkel, "Versatile vacuum packaging for experimental study of resonant MEMS," *2010 IEEE 23rd International Conference on Micro Electro Mechanical Systems (MEMS)*, pp. 516-519, 24-28 Jan. 2010, 2010.
[86] M. Moraja, and M. Amiotti, "Getters films at wafer level for wafer to wafer bonded MEMS," *Symposium on Design, Test, Integration and Packaging of MEMS/MOEMS 2003.*, pp. 346-349, 5-7 May 2003, 2003.
[87] D. R. Sparks, S. Massoud-Ansari, and N. Najafi, "Chip-level vacuum packaging of micromachines using NanoGetters," *Advanced Packaging, IEEE Transactions on,* vol. 26, no. 3, pp. 277-282, 2003.
[88] D. Sparks, S. Massoud-Ansari, and N. Najafi, "Long-term evaluation of hermetically glass frit sealed silicon to Pyrex wafers with feedthroughs," *Journal of Micromechanics and Microengineering,* vol. 15, no. 8, pp. 1560, 2005.
[89] V. O. Tetens, *Zeitschrift fur Geophysik*, no. 6, pp. 297-309, 1930.
[90] M. L. Kidd, "Watch out for those thermoelectric voltages," *Cal Lab: The international journal of metrology*, no. Apr May Jun, pp. 18-21, 2012.
[91] *Low Level Measurements Handbook*, 6th ed.: Keithley Instruments, Inc., 2004.

Articles omitted from online publication due to publishers' restrictions:

1. Å. Sandvand, E. Halvorsen and K.E. Aasmundtveit, "Finite element modelling of influence of bonding material distribution in precision piezoresistive MEMS pressure-sensors", *Electronics System-Integration Technology Conference (ESTC)*, Helsinki, Finland, 16-18 September 2014, DOI: 10.1109/ESTC.2014.6962829

2. Å. Sandvand, E. Halvorsen, K.E. Aasmundtveit and H. Jakobsen, "Influence of sensor-package hermeticity-level on long-term drift for a piezoresistive MEMS pressure-sensor", *Microelectronics Packaging Conference (EMPC)*, Friedrichshafen, Germany, 14-16 September 2015

3. Å. Sandvand, E. Halvorsen, K.E. Aasmundtveit and H. Jakobsen, "Influence of Glass-Frit Material Distribution on the Performance of Precision Piezoresistive MEMS Pressure Sensors", *IEEE Transactions on Components, Packaging and Manufacturing Technology (TCPMT),* Volume 5, Issue 11 (2015), Pages 1559-1566, DOI: 10.1109/TCPMT.2015.2486018

4. Å. Sandvand, E. Halvorsen, K.E. Aasmundtveit and H. Jakobsen, "Identification and elimination of hygro-thermo-mechanical stress-effects in a high-precision MEMS pressure sensor", *IEEE Journal of Microelectromechanical Systems (JMEMS)*, Volume 26, Issue 2 (2017), Pages 415-423, DOI:10.1109/JMEMS.2017.2651162

5. Å. Sandvand, E. Halvorsen and H. Jakobsen, "*In situ* observation of metal properties in a piezoresistive pressure sensor", accepted for publication in *IEEE Journal of Microelectromechanical Systems (JMEMS)* DOI:10.1109/JMEMS.2017.2747090